

1 **Large but decreasing effect of ozone on the European carbon**
2 **sink**

3 Rebecca J Oliver¹, Lina M Mercado^{1,2}, Stephen Sitch², David Simpson^{3,4}, Belinda E Medlyn⁵,
4 Yan-Shih Lin⁵, Gerd A Folberth⁶

5

6 ¹ Centre for Ecology and Hydrology, Benson Lane, Wallingford, OX10 8BB, UK

7 ² College of Life and Environmental Sciences, University of Exeter, EX4 4RJ, Exeter, UK

8 ³ EMEP MSC-W Norwegian Meteorological Institute, PB 43, NO-0313, Oslo, Norway

9 ⁴ Dept. Space, Earth & Environment, Chalmers University of Technology, Gothenburg, SE-41296 Sweden

10 ⁵ Hawkesbury Institute for the Environment, Western Sydney University, Locked Bag 1797, Penrith NSW 2751
11 Australia

12 ⁶ Met Office Hadley Centre, Exeter, UK.

13 *Correspondence to:* Rebecca Oliver (rfu@ceh.ac.uk)

14

15

16

17

18

19

20

21

22

23

24

25

26 **Abstract**

27

28 The capacity of the terrestrial biosphere to sequester carbon and mitigate climate change is governed by the ability
29 of vegetation to remove emissions of CO₂ through photosynthesis. Tropospheric O₃, a globally abundant and
30 potent greenhouse gas, is, however, known to damage plants, causing reductions in primary productivity. Despite
31 emission control policies across Europe, background concentrations of tropospheric O₃ have risen significantly
32 over the last decades due to hemispheric-scale increases in O₃ and its precursors. Therefore, plants are exposed to
33 increasing background concentrations, at levels currently causing chronic damage. Studying the impact of O₃ on
34 European vegetation at the regional scale is important for gaining greater understanding of the impact of O₃ on
35 the land carbon sink at large spatial scales. In this work we take a regional approach and update the JULES land-
36 surface model using new measurements specifically for European vegetation. Given the importance of stomatal
37 conductance in determining the flux of O₃ into plants, we implement an alternative stomatal closure
38 parameterization and account for diurnal variations in O₃ concentration in our simulations. We conduct our
39 analysis specifically for the European region to quantify the impact of the interactive effects of tropospheric O₃
40 and CO₂ on gross primary productivity (GPP) and land carbon storage across Europe. A factorial set of model
41 experiments showed that tropospheric O₃ can suppress terrestrial carbon uptake across Europe over the period
42 1901 to 2050. By 2050, simulated GPP was reduced by 4 to 9% due to plant O₃ damage and land carbon storage
43 by 3 to 7%. The combined physiological effects of elevated future CO₂ (acting to reduce stomatal opening) and
44 reductions in O₃ concentrations resulted in reduced O₃ damage in the future. This alleviation of O₃ damage by
45 CO₂ induced stomatal closure was around 1 to 2% for both land carbon and GPP, depending on plant sensitivity
46 to O₃. Reduced land carbon storage resulted from diminished soil carbon stocks consistent with the reduction in
47 GPP. Regional variations are identified with larger impacts shown for temperate Europe (GPP reduced by 10 to
48 20%) compared to boreal regions (GPP reduced by 2 to 8%). These results highlight that O₃ damage needs to be
49 considered when predicting GPP and land carbon, and that the effects of O₃ on plant physiology need to be
50 considered in regional land carbon cycle assessments.

51

52

53

54

55

56

57

58

59 1 Introduction

60

61 The terrestrial biosphere absorbs around 30% of anthropogenic CO₂ emissions and acts to mitigate climate change
62 (Le Quéré et al., 2015). Early estimates of the European carbon balance suggest a terrestrial carbon sink of between
63 135 to 205 TgC yr⁻¹ (Janssens et al., 2003). Schulze et al. (2009) determined a larger carbon sink of 274 TgC yr⁻¹,
64 and more recent estimates suggest a European terrestrial sink of between 146 to 184 TgC yr⁻¹ (Luysaert et al.,
65 2012). The carbon sink capacity of land ecosystems is dominated by the ability of vegetation to sequester carbon
66 through photosynthesis and release it back to the atmosphere through respiration. Therefore, any change in the
67 balance of these fluxes will alter ecosystem source-sink behaviour.

68

69 In recent decades much attention has focussed on the effects of rising atmospheric CO₂ on vegetation productivity
70 (Ceulemans and Mousseau, 1994;Norby et al., 2005;Norby et al., 1999;Saxe et al., 1998). The Norby et al. (2005)
71 synthesis of Free Air CO₂ Enrichment (FACE) experiments suggests a median stimulation ($23 \pm 2\%$) of forest
72 NPP in response to a doubling of CO₂. Similar average increases (20%) were observed for C₃ crops, although this
73 translated into smaller gains in biomass (17%) and crop yields (13%) (Long et al., 2006). Little attention, however,
74 has been given to tropospheric ozone (O₃), a globally abundant air pollutant recognised as one of the most
75 damaging pollutants for forests (Karlsson et al., 2007;Royal-Society, 2008;Simpson et al., 2014b). Tropospheric
76 O₃ is a secondary air pollutant formed by photochemical reactions involving carbon monoxide (CO), volatile
77 organic compounds (VOCs), methane (CH₄) and nitrogen oxides (NO_x) from both man-made and natural sources,
78 as well as downward transport from the stratosphere and lightning which is a source of NO_x. The phytotoxic
79 effects of O₃ exposure are shown to decrease vegetation productivity and biomass, with consequences for
80 terrestrial carbon sequestration (Felzer et al., 2004;Loya et al., 2003;Mills et al., 2011b;Sitch et al., 2007). Few
81 studies, however, consider the simultaneous effects of exposure to both gases, and few Earth-system models
82 (ESMs) currently explicitly consider the role of tropospheric O₃ in terrestrial carbon dynamics (IPCC, 2013), both
83 of which are important to understanding the carbon sequestration potential of the land-surface, and future carbon
84 dynamics regionally and globally (Le Quéré et al., 2016;Sitch et al., 2015).

85

86 Due to increased anthropogenic precursor emissions over the industrial period, background concentrations of
87 ground-level O₃ have risen (Vingarzan, 2004). Background O₃ is generally defined as the O₃ pollution present in
88 a region that is not attributed to local anthropogenic sources (Vingarzan, 2004). O₃ levels at the start of the 20th
89 century are estimated to be around 10 ppb for the site Montsouris Observatory near Paris, data for Arkona on the
90 Baltic coast increased from ca. 15 ppb in the 1950s to 20-27 ppb by the early 1980s, and the Irish coast site Mace
91 Head shows around 40 ppb by the year 2000 (Logan et al., 2012;Parrish et al., 2012). Present day annual average
92 background O₃ concentrations reported in the review of Vingarzan (2004) show O₃ concentrations range between
93 approximately 20 and 45 ppb, with the greatest increase occurring since the 1950s. Trends vary from site to site
94 though, even on a decadal basis (Logan et al., 2012;Simpson et al., 2014b), depending, for example, on
95 local/regional trends in precursor (especially NO_x) emissions, elevation, and exposure to long-range transport of
96 O₃. Nevertheless, there is some indication that background O₃ levels over the mid-latitudes of the Northern
97 Hemisphere have continued to rise at a rate of approximately 0.5–2% per year, although not uniform (Vingarzan,
98 2004). As a result of controls on precursor emissions in Europe and North America, peak O₃ concentrations in

99 these regions have decreased or stabilised over recent decades (Cooper et al., 2014; Logan et al., 2012; Parrish et
100 al., 2012; Simpson et al., 2014b). Nevertheless, climate change may increase the frequency of weather events
101 conducive to peak O₃ incidents in the future (e.g. summer droughts and heat-waves (Sicard et al., 2013)), and may
102 increase biogenic emissions of the O₃-precursors isoprene and NO_x, although such impacts are subject to great
103 uncertainty (Simpson et al., 2014b; Young et al., 2013; Young et al., 2009). Intercontinental transport of air
104 pollution from regions such as Asia are thought to contribute substantially to rising background O₃ concentrations
105 over the last decades (Cooper et al., 2010; Verstraeten et al., 2015). Northern Hemisphere background
106 concentrations of O₃ are now close to established levels for impacts on human health and the terrestrial
107 environment (Royal-Society, 2008). Therefore, although peak O₃ concentrations are in decline across Europe,
108 plants are exposed to increasing background levels, at levels currently causing chronic damage (Mills et al.,
109 2011b). Intercontinental transport means future O₃ concentrations in Europe will be partly dependent on how O₃
110 precursor emissions evolve globally (Auvray and Bey, 2005; Derwent et al., 2015).

111

112 Rising background O₃ concentrations impact agricultural yields and nutritional quality of major crops (Ainsworth
113 et al., 2012; Avnery et al., 2011), with consequences for global food security (Tai et al., 2014). Increasing
114 background levels of O₃ are damaging to ecosystem health and reduce the global land carbon sink (Arneeth et al.,
115 2010; Sitch et al., 2007). Reduced uptake of carbon by plant photosynthesis due to O₃ damage allows more CO₂
116 to remain in the atmosphere. This effect of O₃ on plant physiology represents an additional climate warming to
117 the direct radiative forcing of O₃, a potent greenhouse gas (Collins et al., 2010; Sitch et al., 2007), the magnitude
118 of which, however, remains highly uncertain (IPCC, 2013).

119

120 Dry deposition of O₃ to terrestrial surfaces, primarily uptake by stomata on plant foliage and deposition on external
121 surfaces of vegetation (Fowler et al., 2001; Fowler et al., 2009), is a large sink for ground level O₃ (Wild,
122 2007; Young et al., 2013). On entry to sub-stomatal spaces, O₃ reacts with other molecules to form reactive oxygen
123 species (ROS). Plants can tolerate a certain level of O₃ depending on their capacity to scavenge and detoxify the
124 ROS (Ainsworth et al., 2012). Above this critical level, long-term chronic O₃ exposure reduces plant
125 photosynthesis and biomass accumulation (Ainsworth, 2008; Ainsworth et al., 2012; Matyssek et al., 2010a; Wittig
126 et al., 2007; Wittig et al., 2009), either directly through effects on photosynthetic machinery such as reduced
127 Rubisco content (Ainsworth et al., 2012; Wittig et al., 2009) and/or indirectly by reduced stomatal conductance
128 (g_s) (Kitao et al., 2009; Wittig et al., 2007), alters carbon allocation to different pools (Grantz et al., 2006; Wittig
129 et al., 2009), accelerates leaf senescence (Ainsworth, 2008; Nunn et al., 2005; Wittig et al., 2009) and changes plant
130 susceptibility to biotic stress factors (Karnosky et al., 2002; Percy et al., 2002).

131

132 The response of plants to O₃ is very wide ranging as reported in the literature from different field studies. The
133 Wittig et al. (2007) meta-analysis of temperate and boreal tree species showed raised O₃ concentrations
134 significantly reduced leaf level light saturated net photosynthetic uptake (-19%, range: -3% to -28% at a mean O₃
135 concentration of 85 ppb) and g_s (-10%, range: +5% to -23% at a mean O₃ concentration of 91 ppb) in both
136 broadleaf and needle leaf tree species. In the Feng et al. (2008) meta-analysis of wheat, O₃ reduced aboveground
137 biomass (-18% at a mean O₃ concentration of 70 ppb) photosynthetic rate (-20% at a mean O₃ concentration of 73
138 ppb) and g_s (-22% at a mean O₃ concentration of 79 ppb). One of few long-term field based O₃ exposure studies

139 (AspenFACE) showed that after 11 years of exposing mature trees to O₃ (mean O₃ concentration of 46 ppb), O₃
140 decreased ecosystem carbon content (-9%), and decreased NPP (-10%), although the O₃ effect decreased through
141 time (Talhelm et al., 2014). Zak et al. (2011) showed this was partly due to a shift in community structure as O₃-
142 tolerant species, competitively inferior in low O₃ environments, out competed O₃-sensitive species. GPP was
143 reduced (-12% to -19%) at two Mediterranean ecosystems exposed to O₃ (ranging between 20 to 72 ppb across
144 sites and through the year) studied by Fares et al. (2013). Biomass of mature beech trees was reduced (-44%) after
145 8 years of exposure to O₃ (~150 ppb) (Matyssek et al., 2010a). After 5 years of O₃ exposure (ambient +20 to +40
146 ppb) in a semi-natural grassland, annual biomass production was reduced (-23%), and in a Mediterranean annual
147 pasture O₃ exposure significantly reduced total aboveground biomass (up to -25%) (Calvete-Sogo et al., 2014).
148 However, these were empirical studies at individual sites, and these focus on O₃ effects on plant physiology and
149 productivity, but do not quantify the impact on the land carbon sink. Modelling studies are needed to scale site
150 observations to the regional and global scales. Models generally suggest that plant productivity and carbon
151 sequestration will decrease with O₃ pollution, though the magnitudes vary. For example, based on a limited dataset
152 to parameterise plant O₃ damage for a global set of plant functional types, Sitch et al. (2007) predicted a decline
153 in global GPP of 14 to 23% by 2100. A second study by Lombardozzi et al. (2015) predicted a 10.8% decrease of
154 present-day (2002-2009) GPP globally. Here we take a regional approach and take advantage of the latest
155 measurements showing changes in plant productivity with accumulated exposure to O₃ specifically for a range of
156 European vegetation from different regions (CLRTAP 2017) with which to calibrate the JULES model for plant
157 sensitivity to O₃, and conduct our analysis specifically for the European region.

158

159 Understanding the response of plants to elevated tropospheric O₃ is challenged by the large variation in O₃
160 sensitivity both within and between species (Karnosky et al., 2007; Kubiske et al., 2007; Wittig et al., 2009).
161 Additionally, other environmental stresses that affect stomatal behaviour will affect the rate of O₃ uptake and
162 therefore the response to O₃ exposure, such as high temperature, drought and changing concentrations of
163 atmospheric CO₂ (Mills et al., 2016; Fagnano et al., 2009; Kitao et al., 2009; Löw et al., 2006). Increasing
164 concentrations of atmospheric CO₂, for example, are suggested to provide some protection against O₃ damage by
165 causing stomata to close (Harmens et al., 2007; Wittig et al., 2007), however the long-term effects of CO₂
166 fertilisation on plant growth and carbon storage remain uncertain (Baig et al., 2015; Ciais et al., 2013). Further, in
167 some studies, stomata have been shown to respond sluggishly, losing their responsiveness to environmental
168 stimuli with exposure to O₃ which can lead to higher O₃ uptake, increased water-loss and therefore greater
169 vulnerability to environmental stresses such as drought (Mills et al., 2016; Mills et al., 2009; Paoletti and Grulke,
170 2010; Wilkinson and Davies, 2009).

171

172 Given the critical role g_s plays in the uptake of both CO₂ and O₃, we use an alternative representation and
173 parameterisation of g_s in JULES by implementing the Medlyn *et al.* (2011) g_s formulation. This model is based
174 on the optimal theory of stomatal behaviour and has advantages over the current JULES g_s formulation of Jacobs
175 (1994) including i) a single parameter (g_1) compared to two parameters in Jacobs (1994), ii) the g_1 parameter is
176 related to the water-use strategy of vegetation and is easier to parameterise with commonly measured leaf or
177 canopy level observations of photosynthesis, g_s and humidity, and (iii) values of g_1 are available for many
178 different plant functional types (PFTs) derived from a global data set of leaf-level measurements (Lin et al., 2015).

179

180 The main objective of this work is to assess the impact of historical and projected (1901 to 2050) changes in
181 tropospheric O₃ and atmospheric CO₂ concentration on predicted GPP and the land-carbon sink for Europe.
182 These are the two greenhouse gases that directly affect plant photosynthesis and g_s . We use a factorial suite of
183 model experiments, using the Joint UK land environment simulator (JULES) (Best et al., 2011; Clark et al.,
184 2011), the land-surface model of the UK Earth System Model (UKESM) (Collins et al., 2011) to simulate plant
185 O₃ uptake and damage, and to investigate the impact of both O₃ and CO₂ on plant water-use and carbon uptake.
186 In this work, the JULES model is re-calibrated using the latest observations of vegetation sensitivity to O₃, with
187 the addition of a separate parameterisation for temperate/boreal regions versus the Mediterranean. The O₃
188 sensitivity of each PFT in JULES was re-calibrated for both a high and low sensitivity to account for uncertainty
189 in the O₃ response, in part due to the observed variation in O₃ sensitivity between species. This includes O₃
190 sensitivities for agricultural crops (wheat – high sensitivity) versus natural grassland (low sensitivity), with
191 separate sensitivities for Mediterranean grasslands. For forests JULES is parameterised with O₃ sensitivities for
192 broadleaf and needle leaf trees (with a high and low O₃ sensitivity for both), with separate sensitivities (high and
193 low) for Mediterranean broadleaf species. We make a separate distinction for the Mediterranean region where
194 possible because the work of Büker et al. (2015) showed that the sensitivity of dominant Mediterranean trees to
195 O₃ is different to temperate species. In addition, we introduce an alternative g_s scheme into JULES as described
196 above. JULES is forced with spatially varying daily O₃ concentrations from a high resolution atmospheric
197 chemistry model for Europe that are disaggregated to hourly concentrations, therefore our simulations account
198 for diurnal variations in O₃ concentration and O₃ responses allowing for improved estimates of O₃ uptake by
199 vegetation. We do not attempt to make a full assessment of the carbon cycle of Europe, instead we target O₃
200 damage, which is currently a missing component in earlier carbon cycle assessments (Le Quéré et al.,
201 2017; Sitch et al., 2015). To this end, we prescribe changing O₃ and CO₂ concentrations from 1901 to 2050, but
202 use a fixed pre-industrial climate. We acknowledge the use of a 'fixed' pre-industrial climate omits the additional
203 uncertainty of the interaction between climate change and g_s which will affect the rate of O₃ uptake and
204 therefore O₃ concentrations. In addition, using uncoupled chemistry and climate is a further source of
205 uncertainty. To understand the impact of these complex feedback mechanisms is an important area for future
206 work, but in the current study our aim is to isolate the physiological response of plants to both O₃ and CO₂, and
207 determine the sensitivity of predicted GPP and the land carbon sink to this process, as the impact of O₃ on the
208 land carbon sink currently remains largely unknown at large spatial scales for Europe.

209

210

211

212 **2 Methods**

213

214 **2.1 Representation of O₃ effects in JULES**

215

216 JULES calculates the land-atmosphere exchanges of heat, energy, mass, momentum and carbon on a sub-daily
217 time step, and includes a dynamic vegetation model (Best et al., 2011; Clark et al., 2011; Cox, 2001). This work
218 uses JULES version 3.3 (<http://www.jchmr.org>) at 0.5° x 0.5° spatial resolution and hourly model time step, the

219 spatial domain is shown in Fig. S1. JULES has a multi-layer canopy radiation interception and photosynthesis
 220 scheme (10 layers in this instance) that accounts for direct and diffuse radiation, sun fleck penetration through the
 221 canopy, inhibition of leaf respiration in the light and change in photosynthetic capacity with depth into the canopy
 222 (Clark et al., 2011; Mercado et al., 2009). Soil water content also affects the rate of photosynthesis and g_s . It is
 223 modelled using a dimensionless soil water stress factor, β , which is related to the mean soil water concentration
 224 in the root zone, and the soil water contents at the critical and wilting point (Best *et al.*, 2011).

225
 226 To simulate the effects of stomatal O_3 deposition on vegetation productivity and water use, JULES uses the flux-
 227 gradient approach of Sitch *et al.*, (2007), modified to include non-stomatal deposition following Tuovinen et al.
 228 (2009). A similar approach is taken by Franz et al. (2017) in the OCN model, however plant O_3 damage is a
 229 function of accumulated O_3 exposure over time. In JULES, plant O_3 damage is instantaneous, because the impact
 230 of cumulative O_3 exposure on plant productivity has already been calibrated with observations (described below).
 231 JULES uses a coupled model of g_s and photosynthesis, the potential net photosynthetic rate (A_p , mol CO_2 m^{-2} s^{-1})
 232 is modified by an ' O_3 uptake' factor (F , the fractional reduction in photosynthesis), so that the actual net
 233 photosynthesis (A_{net} , mol CO_2 m^{-2} s^{-1}) is given by equation 1 (Clark *et al.*, 2011, Sitch *et al.*, 2007). Because of the
 234 relationship between these two fluxes, the direct effect of O_3 damage on photosynthetic rate also leads to a
 235 reduction in g_s . An alternative approach was taken by Lombardozzi et al. (2012) in the CLM model where
 236 photosynthesis and g_s are decoupled, so that O_3 exposure affects carbon assimilation and transpiration
 237 independently. In JULES, changes in atmospheric CO_2 concentration also affect photosynthetic rate and g_s ,
 238 consequently the interactive effects of changing concentrations of both CO_2 and O_3 is allowed for.

239
 240
$$A_{net} = A_p F \tag{1}$$

241
 242 The O_3 uptake factor (F) is defined as:

243
 244
$$F = 1 - a * \max[F_{O_3} - F_{O_3crit}, 0.0] \tag{2}$$

245
 246 F_{O_3} is the instantaneous leaf uptake of O_3 (nmol m^{-2} s^{-1}), F_{O_3crit} is a PFT-specific threshold for O_3 damage (nmol
 247 m^{-2} PLA s^{-1} , projected leaf area), and 'a' is a PFT-specific parameter representing the fractional reduction of
 248 photosynthesis with O_3 uptake by leaves. Following Tuovinen et al. (2009), the flux of O_3 through stomata, F_{O_3} ,
 249 is represented as follows:

250
 251
$$F_{O_3} = O_3 \left(\frac{g_b \left(\frac{g_l}{K_{O_3}} \right)}{g_b + \left(\frac{g_l}{K_{O_3}} \right) + g_{ext}} \right) \tag{3a}$$

252
 253 O_3 is the molar concentration of O_3 at reference (canopy) level (nmol m^{-3}), g_b is the leaf-scale boundary layer
 254 conductance (m s^{-1} , eq 3b), g_l is the leaf conductance for water (m s^{-1}), K_{o_3} accounts for the different diffusivity of
 255 ozone to water vapour and takes a value of 1.51 after Massman (1998), and g_{ext} is the leaf-scale non-stomatal
 256 deposition to external plant surfaces (m s^{-1}) which takes a constant value of 0.0004 m s^{-1} after Tuovinen et al.
 257 (2009). The leaf-level boundary layer conductance (g_b) is calculated as in Tuovinen *et al.* (2009)

258
259
260
261
262
263
264
265
266
267
268
269
270
271
272
273
274
275
276
277
278
279
280
281
282
283
284
285
286
287
288
289
290
291
292
293
294
295
296

$$g_b = \alpha Ld^{-1/2}U^{-1/2} \tag{3b}$$

α is a constant ($0.0051 \text{ m s}^{-1/2}$), Ld is the cross-wind leaf dimension (m) defined per PFT as 0.05 for trees, 0.02 for grasses (C_3 and C_4) and 0.04 for shrubs, U is wind speed at canopy height (m s^{-1}). The rate of O_3 uptake is dependent on g_s , which is dependent on photosynthetic rate. Given g_s is a linear function of photosynthetic rate in JULES (Clark et al., 2011), from eq 1 it follows that:

$$g_s = g_l F \tag{4}$$

The O_3 flux to stomata, F_{O_3} , is calculated at leaf level and then scaled to each canopy layer differentiating sunlit and shaded leaf photosynthesis, and finally summed up to the canopy level. Because the photosynthetic capacity, photosynthesis and therefore g_s decline with depth into the canopy, this in turn affects O_3 uptake, with the top leaf level contributing most to the total O_3 flux and the lowest level contributing least.

2.2 Calibration of O_3 uptake model

Here we use the latest literature on flux based O_3 dose-response relationships derived from observed field data across Europe (CLRTAP, 2017) to determine the key PFT-specific O_3 sensitivity parameters in JULES (a and $F_{\text{O}_3\text{crit}}$). Synthesis of information expressed as O_3 flux based dose-response relationships derived from field experiments is carried out by The United Nations Convention on Long-Range Transboundary Air Pollution (CLRTAP Convention), this information is then used as a policy tool to inform emission reduction strategies in Europe to improve air quality (CLRTAP, 2017; Mills et al., 2011a). Derivation of O_3 flux based dose-response relationships for different vegetation types uses the accumulated stomatal O_3 flux above a threshold (often referred to as the phytotoxic O_3 dose above a threshold of ‘y’ i.e. POD_y) as the dose metric, and the percentage change in biomass as the response metric (Emberson et al., 2007; Karlsson et al., 2007). We use these observation based O_3 dose-response relationships to calibrate each JULES PFT for sensitivity to O_3 using available relationships for the closest matching vegetation type. For JULES, $F_{\text{O}_3\text{crit}}$ is the threshold for O_3 damage, and values for this parameter are taken from the O_3 dose-response relationships as the POD_y value (see CLRTAP, 2017 and Buker et al. 2015 for derivation of POD_y values). The actual sensitivity to O_3 is determined by the slope of the O_3 dose-response relationship, i.e. how much biomass changes with accumulated stomatal uptake of O_3 above the damage threshold, this relates to the parameter a in JULES. The parameter ‘ a ’ is a PFT-specific parameter representing the fractional reduction of photosynthesis with O_3 uptake by leaves. Values for this parameter are found for each PFT by running JULES with different values of ‘ a ’, which alter the instantaneous photosynthetic rate, but then calculating the accumulated stomatal flux of O_3 and the change in productivity, until the slope of this relationship produced by the JULES simulations matches that of the O_3 dose-response relationships derived from observations. Essentially we calibrate each JULES PFT for sensitivity to O_3 by reproducing the observation-based O_3 dose-response relationships.

297 Each PFT was calibrated for high and low plant O₃ sensitivity to account for uncertainty in the sensitivity of
298 different plant species to O₃, using the approach of Sitch *et al.*, (2007). Therefore, when using our results to assess
299 the impact of O₃ at the land surface, we are able to provide a range in our estimates to help address some of the
300 uncertainty in the O₃ response of different vegetation types. In addition, where possible owing to available data,
301 a distinction was made for Mediterranean regions. This was because the work of Bükér *et al.* (2015) showed that
302 different O₃ dose-response relationships are needed to describe the O₃ sensitivity of dominant Mediterranean trees.
303 For the C₃ herbaceous PFT, the dominant land cover type across the European domain in this study (Fig. S2), the
304 high plant O₃ sensitivity was calibrated against observations for wheat to give a representation of agricultural
305 regions and wheat is one of the most sensitive grasses to O₃ (Fig. S3, Table S1). For the low plant O₃ sensitivity
306 JULES was calibrated against the dose-response function for natural grassland to give a representation of natural
307 grassland and this vegetation has a much lower sensitivity to O₃ damage, for the Mediterranean region we used a
308 function for Mediterranean natural grasslands, all taken from CLRTAP (2017) (Fig. S3, Table S1). Tree/shrub
309 PFTs were calibrated against observed O₃ dose-response functions for the high plant O₃ sensitivity: broadleaf
310 trees (temperate/boreal) = Birch/Beech dose-response relationship, broadleaf trees (Mediterranean) = deciduous
311 oaks dose-response relationship, needle leaf trees = Norway spruce dose-response relationship, shrubs =
312 Birch/Beech dose-response relationship, all from CLRTAP (2017) (Fig. S3, Table S1). Data on O₃ dose-response
313 relationships for different vegetation types is very limited, therefore for the low plant O₃ sensitivity calibration for
314 trees/shrubs we assumed a 20% decrease in sensitivity to O₃ based on the difference in sensitivity between high
315 and low sensitive tree species in the Karlsson *et al.* (2007) study. Due to limitations in data availability, the shrub
316 parameterisation uses the observed dose-response functions for broadleaf trees. Similarly, the parameterisation
317 for C₄ herbaceous uses the observed dose-responses for C₃ herbaceous, however the fractional cover of C₄ herbs
318 across Europe is low (Fig. S2), so this assumption affects a very small percentage of land cover.

319
320 To calibrate the JULES O₃ uptake model, JULES was run across Europe forced using the WFDEI observational
321 climate dataset (Weedon, 2013) at 0.5° X 0.5° spatial and three hour temporal resolution. JULES uses interpolation
322 to disaggregate the forcing data down from 3 hours to an hourly model time step. The model was spun-up over
323 the period 1979 to 1999 with a fixed atmospheric CO₂ concentration of 368.33 ppm (1999 value from Mauna Loa
324 observations (Tans and Keeling, 2014)). Zero tropospheric ozone concentration was assumed for the control
325 simulation, for the simulations with O₃, spin-up used spatially explicit fields of present day O₃ concentration
326 produced using the UK Chemistry and Aerosol (UKCA) model with standard chemistry from the run evaluated
327 by O'Connor *et al.* (2014). A fixed land cover map was used based on IGBP (International Geosphere-Biosphere
328 Programme) land cover classes (IGBP-DIS), therefore as the vegetation distribution was fixed and the calibration
329 was not looking at carbon stores, a short spin-up was adequate to equilibrate soil temperature and soil moisture.
330 JULES was then run for the year 2000 with a corresponding CO₂ concentration of 369.52 ppm (from Mauna Loa
331 observations (Tans and Keeling, 2014)) and monthly fields of spatially explicit tropospheric O₃ (O'Connor *et al.*,
332 2014) as necessary.

333
334 Calibration was performed using four simulations: with i) zero tropospheric O₃ concentration, this was the control
335 simulation (control), ii) tropospheric O₃ at current ambient concentration (O3), iii) ambient +20 ppb (O3+20) and
336 iv) ambient +40 ppb (O3+40). The different O₃ simulations (i.e. O3, O3+20 and O3+40) were used to capture the

337 range of O₃ conditions in the data used in the observation-based O₃ dose-response relationships used in this study
 338 for calibration, often data were from experiments using artificially manipulated conditions of ambient + 40 ppb
 339 O₃ for example. For each JULES O₃ simulation, the value of F_{O_3crit} was taken from the vegetation specific O₃
 340 dose-response relationship as the threshold O₃ concentration above which damage to vegetation occurs. An initial
 341 estimate of the parameter ‘a’ was used, then for each PFT and each simulation, hourly estimates of NPP (our
 342 proxy for biomass – although not identical they are related) and O₃ uptake in excess of F_{O_3crit} were accumulated
 343 over a PFT dependent accumulation period. The accumulation periods were ~6 months for broadleaf trees and
 344 shrubs, all year for needle leaf trees, and ~3 months for herbaceous species, through the growing season, following
 345 guidelines in CLRTAP (2017). Additionally, in accordance with the methods used in the CLRTAP (2017) that
 346 describe how the O₃ dose-response relationships are derived from observations, we use the stomatal O₃ flux per
 347 projected leaf area to top canopy sunlit leaves. The percentage change in total NPP was calculated for each O₃
 348 simulation and plotted against the cumulative uptake of O₃ over the PFT-specific accumulation period. The linear
 349 regression of this relationship was calculated, and slope and intercept compared against the slope and intercept of
 350 the observed dose-response relationships. Values of the parameter ‘a’ were adjusted, and the procedure repeated
 351 until the linear regression through the simulation points matched that of the observations (Fig. S3, Table S1).

352

353 2.3 Representation of stomatal conductance and site level evaluation

354

355 In JULES, g_s (m s⁻¹) is represented following the closure proposed by (Jacobs, 1994):

356

$$357 \quad g_s = 1.6RT_l \frac{A_{net}\beta}{c_a - c_i} \quad (5)$$

358

359 In this parameterisation, c_i is unknown and in the default JULES model is calculated as in equation 6, hereafter
 360 called JAC:

361

$$362 \quad c_i = (c_a - c_*)f_0 \left(1 - \frac{dq}{dq_{crit}}\right) + c_* \quad (6)$$

363

364 β is a soil moisture stress factor, the factor 1.6 accounts for g_s being the conductance for water vapour rather than
 365 CO₂, R is the universal gas constant (J K⁻¹ mol⁻¹), T_l is the leaf surface temperature (K), c_a and c_i (both Pa) are the
 366 leaf surface and internal CO₂ partial pressures, respectively, c_* (Pa) is the CO₂ photorespiration compensation
 367 point, dq is the humidity deficit at the leaf surface (kg kg⁻¹), dq_{crit} (kg kg⁻¹) and f_0 are PFT specific parameters
 368 representing the critical humidity deficit at the leaf surface, and the leaf internal to atmospheric CO₂ ratio (c_i/c_a)
 369 at the leaf specific humidity deficit (Best *et al.* 2011), values are shown in Table S1.

370

371 In this work, we replace equation 6 with the closure described in Medlyn *et al.* (2011), using the key PFT specific
 372 model parameter g_l (kPa^{0.5}), and dq is expressed in kPa, shown in eq 7, hereafter called MED:

373

$$374 \quad c_i = c_a \left(\frac{g_l}{g_l + \sqrt{dq}} \right) \quad (7)$$

375

376 PFT specific values of the g_l parameter were derived for European vegetation from the data base of Lin et al.
377 (2015) and are shown in Table S1. The g_l parameter represents the sensitivity of g_s to the assimilation rate, i.e.
378 plant water use efficiency, and was derived as in Lin et al. (2015) by fitting the Medlyn *et al.*, (2011) model to
379 observations of g_s , photosynthesis, and VPD, assuming an intercept of zero.

380

381 The impact of g_s model formulation (JAC versus MED) on simulated water, O_3 , carbon and energy fluxes is
382 compared for two contrasting grid points - wet (low soil moisture stress) and dry (high soil moisture stress) in the
383 European domain. JULES was spun-up for 20 years (1979-1999) at two grid points in central Europe representing
384 a wet (low soil moisture stress, lat: 48.25; lon:, 5.25) and a dry site (high soil moisture stress, lat: 38.25; lon:, -
385 7.75). The modelled soil moisture stress factor ($fsmc$) at the wet site ranged from 0.8 to 1.0 over the year 2000
386 (1.0 indicates no soil moisture stress), and at the dry site $fsmc$ steadily declined from 0.8 at the start of the year to
387 0.25 by the end of the summer. The WFDEI meteorological forcing dataset was used (Weedon, 2013), along with
388 atmospheric CO_2 concentration for the year 1999 (368.33 ppm), and either no O_3 (i.e. the O_3 damage model was
389 switched off) for the control simulations, or spatially explicit fields of present day O_3 concentration produced
390 using the UK Chemistry and Aerosol (UKCA) model from the run evaluated by O'Connor et al. (2014) for the
391 simulations with O_3 . Following the spin-up period, JULES was run for one year (2000) with corresponding
392 atmospheric CO_2 concentration, and tropospheric O_3 concentrations as described above. The control and O_3
393 simulations were performed for both JAC and MED model formulations. Land cover for the spin-up and main run
394 was fixed at 20% for each PFT. For the simulations including O_3 damage, the high plant O_3 sensitivity
395 parameterisation was used. The difference between these simulations was used to assess the impact of g_s model
396 formulation on the leaf level fluxes of carbon and water. We calculate and report (results section 3.1) the difference
397 in mean annual water-use that results from the above simulations using the different g_s models. For each day of
398 the simulation we calculate the percentage difference in water-use between the two simulations, we then calculate
399 the mean and standard deviation over the year to give the annual mean leaf-level water-use.

400

401 Site level evaluation of the two g_s models compared to FLUXNET observations was carried out to evaluate the
402 seasonal cycles of latent and sensible heat using the two g_s models JAC and MED compared to observations.
403 Seven Fluxnet towers were selected to represent a range of land cover types as shown in Table S2. JULES was
404 setup for each site using observed site-level hourly meteorology, and the vegetation cover was prescribed
405 according to the fractional covers of the different JULES surface types shown in Table S2. Following a spin-up
406 period, simulations were run at each site for the years shown in Table S2.

407

408 **2.4 Model simulations for Europe**

409

410 **2.4.1 Forcing datasets**

411

412 We used the WATCH meteorological forcing data set (Weedon et al., 2010; Weedon et al., 2011) at $0.5^\circ \times 0.5^\circ$
413 spatial and three hour temporal resolution for our JULES simulations. JULES interpolates this down to an hourly

414 model time step. For this study, the climate was kept constant by recycling over the period 1901 to 1920, to allow
415 us to focus on the impact of O₃, CO₂ and their interactive effects.

416

417 JULES was run with prescribed annual mean atmospheric CO₂ concentrations. Pre-industrial global CO₂
418 concentrations (1900 to 1960) were taken from Etheridge et al. (1996), 1960 to 2002 were from Mauna Loa
419 (Keeling and Whorf, 2004), as calculated by the Global Carbon Project (Le Quéré et al., 2016), and 2003-2050
420 were based on the IPCC SRES A1B scenario and were linearly interpolated to gap fill missing years (Fig. 1).

421

422 JULES was run including dynamic vegetation with a land cover mask giving the fraction of agriculture in each
423 0.5° x 0.5° grid cell based on the Hurtt et al. (2011) land cover database for the year 2000. The agricultural mask
424 is fixed and does not change over the simulation period. This means that whilst the model is allowed to evolve its
425 own vegetation cover outside of the agricultural mask, within the mask only C₃/C₄ herbaceous PFTs are allowed
426 to grow, with no competition from other PFTs. Therefore, through the simulation period, regions of agriculture
427 are maintained as such and not out-competed by forests for example, allowing for a more accurate representation
428 of the land cover of Europe in the model. No form of land management is simulated (i.e. no crop harvesting,
429 ploughing, rotation or grazing), growth and leaf area index (LAI) are determined by resource availability and
430 phenology. Outside of the agricultural mask, dynamic vegetation means that grid cell PFT coverage and LAI are
431 the result of resource availability, phenology and simulated competition. Across the model domain, simulated
432 mean annual LAI was dominantly within the range of 2 to 5 m²/m² (Fig. S4 and S5). Following a full spin-up
433 period (to ensure equilibrium vegetation, carbon and water states), there was no significant change in the fractional
434 cover of each PFT over the simulation period (1901 - 2050). By 2050, increases in boreal forest cover occurred,
435 but this was less than 2% and limited to very small areas, given this small change we show just the land cover for
436 2050 in Fig. S2.

437

438 Tropospheric O₃ concentration was produced by the EMEP MSC-W model at 0.5° x 0.5° (Simpson et al., 2012),
439 driven with meteorology from the regional climate model RCA3 (Kjellström et al., 2011; Samuelsson et al., 2011),
440 which provides a downscaling of the ECHAM A1B-r3 (simulation 11 of Kjellström *et al.*, 2011). This setup
441 (EMEP+RCA3) is also used by Langner et al. (2012a), Simpson et al. (2014a), Tuovinen et al. (2013), Franz et
442 al. (2017) and Engardt et al. (2017), where further details and model evaluation can be found. Unfortunately, the
443 3-dimensional RCA3 data needed by the EMEP model was not available prior to 1960, but as in Engardt et al.
444 (2017) the meteorology of 1900-1959 had to be approximated by assigning random years from 1960 to 1969. This
445 procedure introduces some uncertainty of course, although Langner et al. (2012b) show that for the period 1990
446 to 2100 it is emissions change, rather than meteorological change, that drives modelled O₃ concentrations. The
447 emissions scenarios for 1900-2050 merge data from the International Institute of Applied System Analysis
448 (IIASA) for 2005-2050 (the so-called ECLIPSE 4a scenario), recently revised EMEP data for 1990, and a scaling
449 back from 1990 to 1900 using data from Lamarque et al. (2013). The trend in emissions of the major O₃ precursors
450 NO_x, NMVOC and Isoprene are shown from 1900 to 2050 over Europe in Fig. S6. Isoprene emissions are not
451 inputs to the EMEP model, but rather calculated at each time-step using temperature, radiation, and land-cover
452 specific emission factors (Simpson et al., 2012). Changes in the assumed background concentration of CH₄ (from
453 RCP6.0) (van Vuuren et al., 2011) are also shown in Fig. S6. Engardt et al. (2017) show the trend in emissions of

454 SO₂ and NH₃ from 1900 to 2050 over Europe. The EMEP model accounts for changes in BVOC emissions as a
455 result of predicted ambient temperature changes.

456

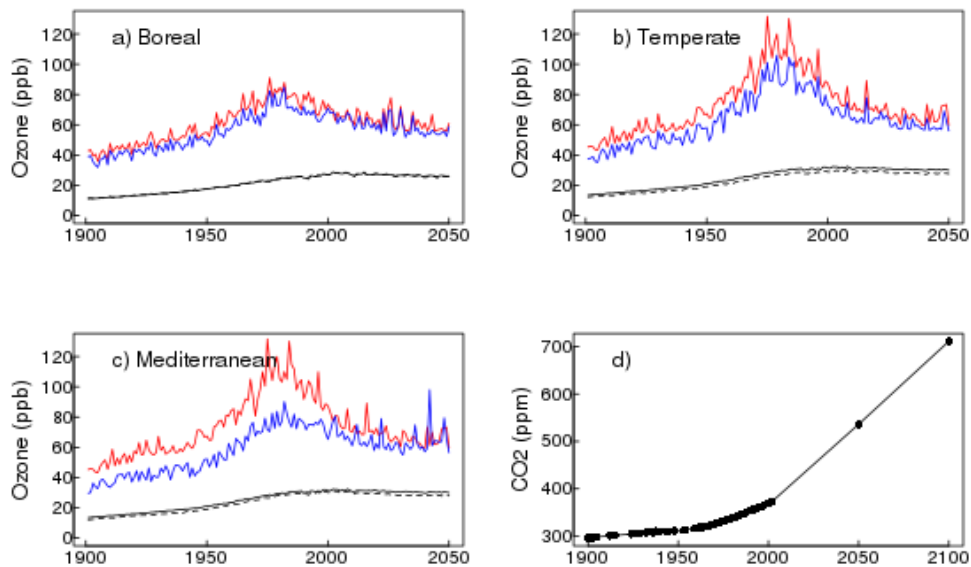
457 O₃ concentrations from EMEP MSC-W were calculated at canopy height for two land-cover categories: forest
458 and grassland (Fig. S7 and Fig. S8), which are taken as surrogates for high and low vegetation, respectively. These
459 canopy-height specific concentrations allow for the large gradients in O₃ concentration that can occur in the lowest
460 10s of metres, giving lower O₃ for grasslands than seen at e.g. 20 m in a forest canopy (Gerosa et al., 2017; Simpson
461 et al., 2012; Tuovinen et al., 2009). These canopy level O₃ concentrations are used as input to JULES, using the
462 EMEP O₃ concentrations for forest for the forest JULES PFTs (broadleaf/needle leaf tree and shrub), and the
463 EMEP O₃ concentrations for grassland for the grass/herbaceous JULES PFTs (C₃ and C₄). This study used daily
464 mean values of tropospheric O₃ concentration from EMEP disaggregated down to the hourly JULES model time-
465 step. The daily mean O₃ forcing was disaggregated to follow a mean diurnal profile of O₃, this was generated from
466 hourly O₃ output from EMEP MSC-W for the two land cover categories (forest and grassland as described above)
467 across the same model domain. O₃ concentrations follow a diurnal cycle and peak during the day, therefore
468 accounting for the diurnal variation in O₃ concentrations allows for a more realistic estimation of O₃ uptake.

469

470 Figure 1 shows large increases in tropospheric O₃ from pre-industrial to present day (2001), this is in line with
471 modelling studies (Young et al., 2013) and site observations (Derwent et al., 2008; Logan et al., 2012; Parrish et
472 al., 2012), and is predominantly a result of increasing anthropogenic emissions (Young et al., 2013). Figures S7
473 and S8 show this large increase in ground-level O₃ concentrations from 1901 to 2001 occurs in all seasons. Present
474 day O₃ concentration show a strong seasonal cycle, with a spring/summer peak in concentrations in the mid-
475 latitudes of the Northern Hemisphere (Derwent et al., 2008; Parrish et al., 2012; Vingarzan, 2004). Seasonal cycles
476 have been changing over the past decades however, attributed to changes in NO_x and other emissions, as well as
477 changes in transport patterns (Parrish et al., 2013). These changes will likely continue in future as emissions and
478 meteorological factors impact photo-chemical O₃ production and transport patterns. Indeed, the O₃ concentrations
479 used in the simulations in this study show increased O₃ levels in winter and in some regions in autumn and spring
480 in 2050 compared to present day, this may be due to reduced titration of O₃ by NO as a result of reduced NO_x
481 emissions in the future (Royal Society, 2008). Summer O₃ concentrations are lower in 2050 however, compared
482 to 2001.

483

484



485

486 **Figure 1.** Regional time series of canopy height O₃ (ppb) forcing from EMEP a) to c), and d) global atmospheric
 487 CO₂ (ppm) concentration (this does not vary regionally; black dots show data points, the black line shows
 488 interpolated points). Each panel for the O₃ forcing shows the regional annual average (woody PFTs, black solid
 489 line; herbaceous PFTs, black dashed line) and the annual maximum O₃ concentration above: woody PFTs (red)
 490 and herbaceous PFTs (blue).

491

492 2.4.2 Spin up and factorial experiments

493

494 JULES was spun-up by recycling the climate from the early part of the twentieth century (1901 to 1920) using
 495 atmospheric CO₂ (296.1 ppm) and O₃ concentrations from 1901 (Fig. S7 & Fig. S8). Model spin-up was 2000
 496 years by which point the carbon pools and fluxes were in steady state with zero mean net land – atmosphere CO₂
 497 flux. We performed the following transient simulations for the period 1901 to 2050 with continued recycling of
 498 the climate as used in the spin-up, for both high and low plant O₃ sensitivities:

499

- 500 • **run_O3** : Fixed 1901 CO₂, Varying O₃
- 501 • **run_CO2** : Varying CO₂, Fixed 1901 O₃
- 502 • **run_both_CO2+O3** : Varying CO₂, Varying O₃

503

504 We use these simulations to investigate the direct effects of changing atmospheric CO₂ and O₃ concentrations,
 505 individually and combined, on plant water-use, GPP and the land C sink through the twentieth century and into
 506 the future, specifically over three time periods: historical (1901-2001), future (2001-2050) and over the full time
 507 series (1901-2050). For each time period we calculate the difference between the decadal means calculated at the
 508 start and end of the analysis period for each variable of interest. Therefore our results report the change in GPP,
 509 for example, over the analysis period. For each variable analysed (GPP, NPP, vegetation carbon, soil carbon, total
 510 land carbon and *g_s*), we use the mean over 10 years to represent each time period, e.g. the mean over 2040 to 2050
 511 is what we call 2050, 1901 to 1910 is what we refer to as 1901. The difference between the simulations gives the
 512 effect of O₃ and CO₂ either separately or in combination over the different time periods. We look at the percentage

513 change due to either O₃ at pre-industrial CO₂ concentration (i.e. without the additional effect of atmospheric CO₂
514 on stomatal behaviour – run_O3), CO₂ (at fixed pre-industrial O₃ concentration, run_CO2) or the combined effect
515 of both gases (run_both_CO2+O3), e.g. $100 * (\text{varO}_3[2050] - \text{varO}_3[1901]) / \text{varO}_3[1901]$ gives the O₃ effect (at
516 fixed CO₂) over the full experimental period. The meteorological forcing is prescribed in these simulations and is
517 therefore the same between the model runs. Other climate factors, such as VPD, temperature and soil moisture
518 availability are accounted for in our simulations, but our analysis isolates the effects of O₃, CO₂ and O₃ + CO₂.
519 We also use paired t-test to determine statistically significant differences between the different (high and low)
520 plant O₃ sensitivities.

521

522 2.4.3 Evaluation

523 To evaluate our JULES simulations we compare mean GPP from 1991 to 2001 for each of the JULES scenarios
524 and both high and low plant O₃ sensitivities against the observation based globally extrapolated Flux Network
525 model tree ensemble (MTE) (Jung et al., 2011). We use paired t-test to determine statistically significant
526 differences in the mean responses.

527

528 3 Results

529

530 3.1 Impact of g_s model formulation and site level evaluation

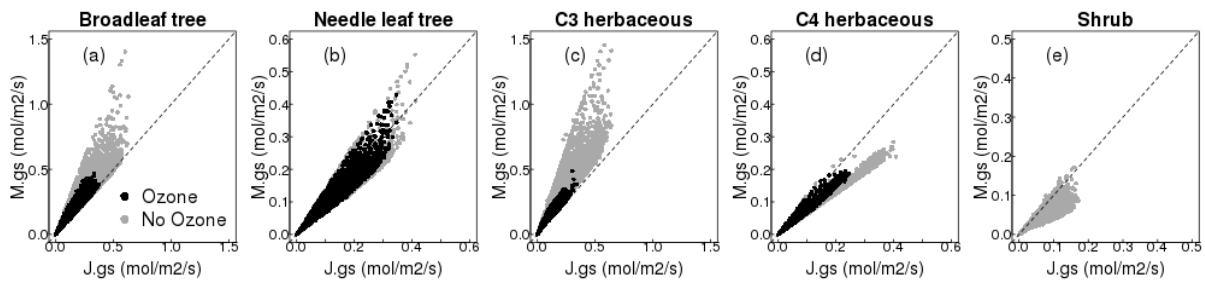
531

532 The impact of g_s model on simulated g_s is shown for the site with low soil moisture stress (wet site, Fig. 2). For
533 the broadleaf tree and C₃ herbaceous PFT, the MED model simulates a larger conductance compared to the JAC
534 model. In other words, with the MED model these two PFTs are parameterised with a less conservative water use
535 strategy, which, for the grid point shown in Fig. 2, increased the annual mean water use by 35% (±29%) and 45%
536 (±32%), respectively. In contrast, the needle leaf tree, C₄ herbaceous and shrub PFTs are parameterised with a
537 more conservative water use strategy with the MED model, and the mean annual g_s was decreased by 13% (±12%),
538 27% (±10%) and 36% (±13%), respectively, compared to the JAC model. This comparison was also done for a
539 dry site (high soil moisture stress), and similar results were found (Fig. S9). The effect of g_s formulation on
540 simulated photosynthesis was much smaller because of the lower sensitivity of the limiting rates of photosynthesis
541 to changes in c_i in the model compared to the effect of the same change in c_i on modelled g_s (Fig. S10 & S11).
542 Changes in g_s impact the partitioning of simulated energy fluxes. In general, increased g_s results in increased latent
543 heat and thus decreased sensible heat flux, and vice versa where g_s is decreased (Fig. S10 & S11). Also shown is
544 the effect of the MED model on O₃ flux into the leaf (Fig. S12 and Fig. S9 bottom panel). For the broadleaf tree
545 and C₃ herbaceous PFT, the MED model simulates a larger conductance and therefore a greater flux of O₃ through
546 stomata compared to JAC, and this is indicative of the potential for greater reductions in photosynthesis (Fig. S10
547 & S11 top row). The reverse is seen for the needle leaf tree, C₄ herbaceous and shrub PFTs.

548

549 Site level evaluation of the seasonal cycles of latent and sensible heat with both JAC and MED models compared
550 to FLUXNET observations showed in general, the MED model improved the seasonal cycle of both fluxes (lower
551 RMSE), but the magnitude of this varied from site to site (Fig. S13). At the deciduous broadleaf site, US-UMB,

552 MED resulted in improvements of the simulated seasonal cycle particularly in the summer months for both fluxes
 553 (RMSE decreased from 42.7/31.5 to 38.5/28.0 W/m² for latent/sensible heat respectively). At the second
 554 deciduous broadleaf site IT-CA1 however, there was almost no difference between the two g_s models. Both
 555 evergreen needle leaf forest sites (FI-Hyy and DE-Tha) saw improvements in the simulated seasonal cycles of
 556 latent and sensible heat with the MED model, primarily as a result of lower latent heat flux in the spring and
 557 summer months, and higher sensible heat flux over the same period. At FI-Hyy, RMSE decreased from 10.1/7.4
 558 to 6.7/6.7 W/m² for latent/sensible heat respectively, and at DE-Tha, RMSE decreased from 16.0/11.9 to 10.5/10.6
 559 W/m² for latent/sensible heat respectively. With the MED model the monthly mean latent heat flux was improved
 560 at the C₃ grass site (CH-Cha) as a result of increased flux in the summer months (RMSE decreased from 15.7 to
 561 13.8 W/m²), however there was no improvement in the sensible heat flux and RMSE with MED was increased
 562 (from 3.9 to 4.9 W/m²). At the C₄ grass site (US-SRG), small improvements were made in the seasonal cycle of
 563 both latent and sensible heat with the MED model. At the deciduous savannah site (CG-Tch) which included a
 564 high proportion of shrub PFT in the land cover type used in the site simulation, large improvements in the seasonal
 565 cycle of both fluxes were simulated with the MED model, as a result of a decrease in the latent heat flux and an
 566 increase in the sensible heat flux (RMSE decreased from 39.5/31.6 to 30.4/24.4 W/m² for latent/sensible heat
 567 respectively).



568

569 **Figure 2.** Comparison of simulated g_s with MED (y axis) versus JAC (x axis) for all five JULES PFTs at one grid
 570 point (lat: 48.25; lon: 5.25) shown are hourly values for the year 2000 (see SI section S3 for further details).

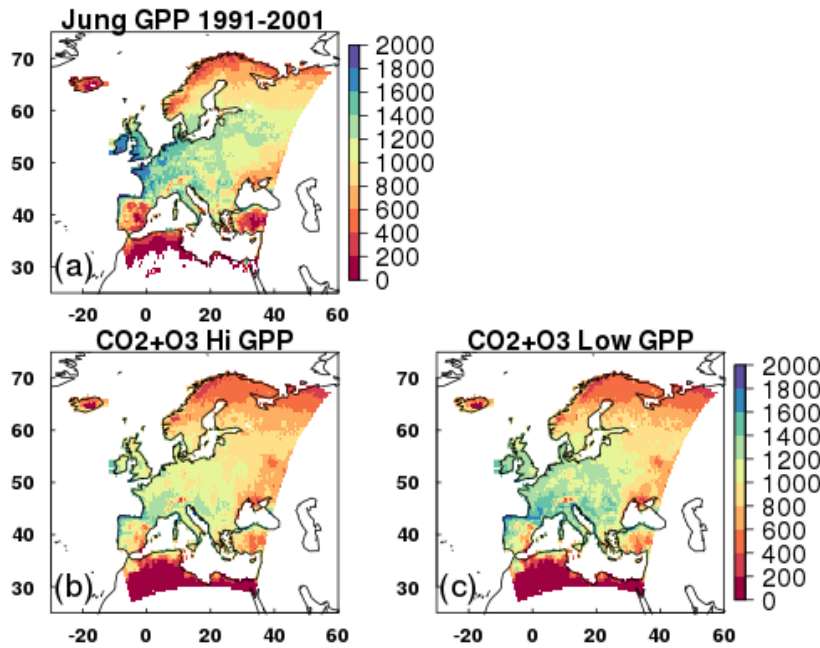
571

572 3.2 Evaluation of the JULES O₃ model

573 For all JULES scenarios similar spatial patterns of GPP are simulated compared to MTE (Fig. 3 and Fig. S14).
 574 MTE estimates a mean GPP for present day in Europe of 938 gC m² yr⁻¹ (Fig. 3). JULES tends to under-predict
 575 GPP relative to the MTE product, estimates of GPP from JULES with both transient CO₂ and O₃
 576 (run_both_CO2+O3) gives a mean across Europe of 813 gC m² yr⁻¹ (high plant O₃ sensitivity) to 881 gC m² yr⁻¹
 577 (low plant O₃ sensitivity), both of which are significantly different to the MTE product ($t=27, d.f.=5750, p<2.2e^{-16}$ (high);
 578 $t=4.3, d.f.=5750, p<1.5e^{-05}$ (low); Fig. 3). Forcing with CO₂ alone (run_CO2) gives a mean GPP across
 579 Europe of 900 to 923 gC m² yr⁻¹ (high and low plant O₃ sensitivity respectively), and O₃ alone (run_O3 - without
 580 the protective effect of CO₂) reduces estimated GPP to 732 to 799 gC m² yr⁻¹ (Fig. S14). At latitudes >45°N JULES
 581 has a tendency to under-predict MTE-GPP, and at latitudes <45°N JULES tends to over-predict MTE-GPP (Fig.
 582 S15). These regional differences are highlighted in Fig. S16, where in the Mediterranean region, JULES tends to
 583 over-predict compared to MTE-GPP, so simulations with O₃ reduce the simulated GPP bringing it closer to MTE.

584 In the temperate region however, JULES tends to under-estimate MTE-GPP, so the addition of O₃ reduces
 585 simulated GPP further (Fig. S16). In the boreal region, JULES under-predicts GPP, but to a lesser extent than in
 586 the temperate region, and the addition of O₃ has less impact on reducing the GPP further (Fig. S16).

587



588

589 **Figure 3.** Mean GPP ($\text{g C m}^2 \text{ yr}^{-1}$) from 1991 to 2001 for a) the observationally based globally extrapolated Flux
 590 Network model tree ensemble (MTE) (Jung *et al.*, 2011); b, c) model simulations with transient CO₂ and transient
 591 O₃ (run_both_CO2+O3), high and low plant O₃ sensitivity respectively.

592

593

594 3.3 European simulations - Historical Period: 1901-2001

595

596 Over the historical period (1901-2001), run_O₃ reduced GPP under both the low and high plant O₃ sensitivity
 597 parameterizations by -3% to -9% respectively (Table 1), and this difference in simulated GPP was significant
 598 ($t=102.2$, $df=6270$, $p<2.2e^{-16}$). Figure 4 highlights regional variations, however, where simulated reductions in
 599 GPP are up to 20% across large areas of Europe, and up to 30% in some Mediterranean regions under the high
 600 plant O₃ sensitivity. Some Boreal and Mediterranean regions show small increases in GPP over this period,
 601 associated with O₃ induced stomatal closure enhancing water availability in these drier regions (Fig. 5). This
 602 allows for greater stomatal conductance later in the year when soil moisture may otherwise have been limiting to
 603 growth (up to 10%, Fig. 5), and therefore higher GPP, but these regions comprise only a small area of the entire
 604 domain. Indeed, over much of the Europe, O₃-induced stomatal closure led to reduced g_s (up to 20%) across large
 605 areas of temperate Europe and the Mediterranean, and even greater reductions in some smaller regions of southern
 606 Mediterranean (Fig. 6), and these are not associated with notable increases in soil moisture availability (Fig. 5),
 607 resulting in depressed GPP over much of Europe as described above. Under the low plant O₃ sensitivity, similar

608 spatial patterns occur, but the magnitude of GPP change (up to -10% across much of Europe) and g_s change (-5%
609 to -10%) are lower compared to the high sensitivity. Over the twentieth century the land carbon sink is suppressed
610 (-2% to -6%, Table 1). Large regional variation is shown in Figure 4, with temperate and Mediterranean Europe
611 seeing a large reduction in land carbon storage, particularly under the high plant O₃ sensitivity (up to -15%).

612

613 Combined, the physiological response to changing CO₂ and O₃ concentrations (run_both_CO2+O3) results in a
614 net loss of land carbon over the twentieth century under the high plant O₃ sensitivity (-2%, Table 1), dominated
615 by loss of soil carbon (Table S3). This reflects the large increases in tropospheric O₃ concentration observed over
616 this period (Fig. 1). Under the low plant O₃ sensitivity, the land carbon sink has started to recover by 2001 (+1.5%)
617 owing to the recovery of the soil carbon pool beyond 1901 values over this period (Table S3).

618

619 To gain perspective on the magnitude of the O₃ induced flux of carbon from the land to the atmosphere we relate
620 changes in total land carbon to carbon emissions from fossil fuel combustion and cement production for the EU-
621 28-plus countries from the data of Boden et al. (2013). We recognise that our simulation domain is slightly larger
622 than the EU28-plus as it includes a small area of western Russia so direct comparisons cannot be made, but this
623 still provides a useful measure of the size of the carbon flux. For the period 1970 to 1979 the simulated loss of
624 carbon from the European terrestrial biosphere due to O₃ effects on vegetation physiology was on average 1.32
625 Pg C (high vegetation sensitivity) and 0.71 Pg C (low vegetation sensitivity) (Table 2). This O₃ induced reduced
626 C uptake of the land surface is equivalent to around 8% to 16% of the emissions of carbon from fossil fuel
627 combustion and cement production over the same period for the EU28-plus countries (Table 2). Currently the
628 emissions data availability goes up to 2011, over the last observable decade (2002 to 2011) the simulated reduction
629 in land carbon due to O₃ has declined, but is still equivalent to 2% to 4% of the emissions of carbon from fossil
630 fuels and cement production for the EU28-plus countries (Table 2). By comparison with one of the largest
631 anthropogenic emissions of carbon for Europe, we show here the potential effect of O₃ on reducing the size of the
632 European land carbon sink is notable.

633

634 **3.4 European simulations - Future Period: 2001-2050**

635

636 Over the 2001 to 2050 period, region-wide GPP with O₃ only changing (run_O3) increased marginally (+0.1% to
637 +0.2%, high and low plant O₃ sensitivity, Table 1, with a significant difference between the two plant O₃
638 sensitivities ($t=57$, $d.f.=6270$ $p<2.2e^{-16}$)), although with large spatial variability as discussed below (Fig. 4g & h).
639 Figures S7 and S8 show that despite decreased tropospheric O₃ concentrations by 2050 in summer compared to
640 2001 levels, all regions are exposed to an increase in O₃ over the wintertime, and some regions of Europe,
641 particularly temperate/Mediterranean experience increases in O₃ concentration in spring and autumn. Therefore,
642 although in the O₃ simulation, overall simulated GPP for Europe shows a small increase, large spatial variability
643 is shown in Fig's 4g & h because of the variability in O₃ concentration with region and season. Increased GPP
644 (dominantly 10%, but up to 20% in some areas) on 2001 levels is simulated across areas of Europe, however,
645 decreases of up to 21% are simulated in some areas of the Mediterranean, up to 15% in some areas of the boreal
646 region and up to 27% in the temperate zone (Fig. 4g & h).

647

648 When O₃ and CO₂ effects are combined (run_both_CO2+O3), simulated GPP increases (+15% to +18%, high/low
649 plant O₃ sensitivities respectively, Table 1). This increase is greater than the enhancement simulated when CO₂
650 affects plant growth independently (run_CO2), because additional O₃ induced stomatal closure increases soil
651 water availability in some regions, which enhances growth more in run_both_CO2+O3, compared to run_CO2.
652 Nevertheless, although the percentage gain is larger, the absolute value of GPP by 2050 remains lower in
653 run_both_CO2+O3 compared to GPP in run_CO2, highlighting the negative impact of O₃ at the land surface
654 (Table S4).

655

656 Despite small increases in GPP in run_O3, the land carbon sink continues to decline from 2001 levels (-0.7% to -
657 1.6%, low and high plant O₃ sensitivity respectively, Table 1). This is because the soil and vegetation carbon pools
658 continue to lose carbon as they adjust slowly to small changes in input (GPP), i.e. the soil carbon pool is not in
659 equilibrium in 2001, and is declining in response to reduced litter input as a result of 20th C O₃ impacts on GPP.
660 Nevertheless, the negative effect of O₃ on the future land sink is markedly reduced relative to the historical period.
661 Figure 4e & f however highlights regional differences. Boreal regions and parts of central Europe see minimal O₃
662 damage, whereas some areas of southern and northern Europe see further losses of up to 8% on 2001 levels. The
663 run_both_CO2+O3 simulation is dominated by the physiological effects of changing CO₂, with land carbon sink
664 increases of up to 7% (Table 1).

665

666 **3.5 European simulations – Full experimental period: 1901-2050**

667

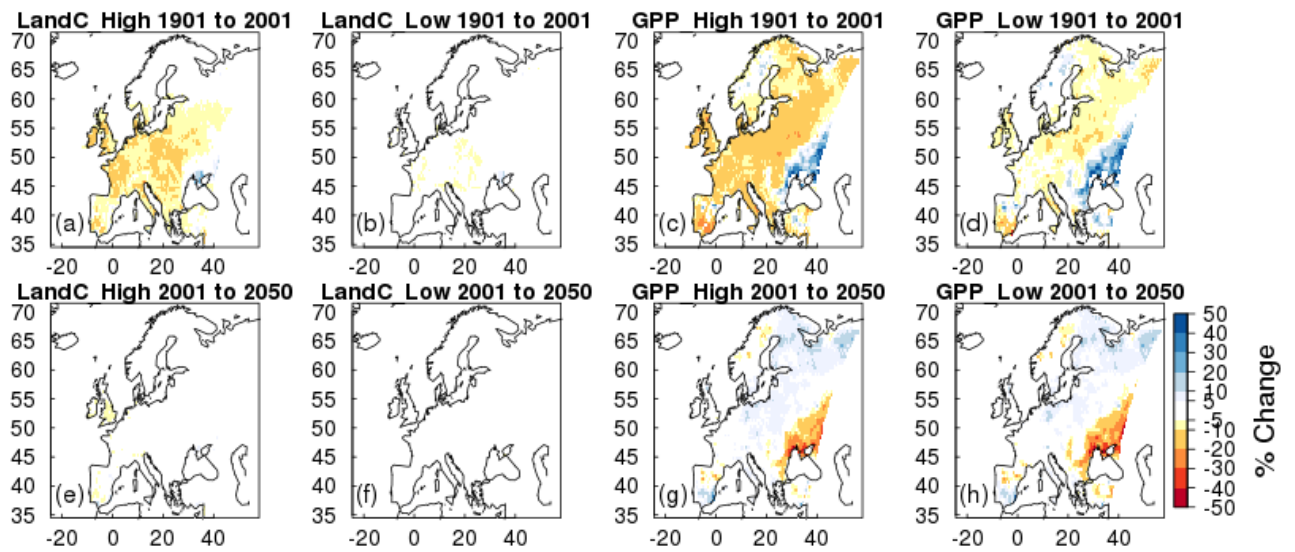
668 From 1901 to 2050, run_O3 reduces GPP (-4% to -9%, with a significant difference between the low and high
669 plant O₃ sensitivity ($t=95$, $d.f.=6270$ $p<2.2e^{-16}$)) and land carbon storage (-3% to -7%, Table 1). Regionally, O₃
670 damage is lowest in the boreal zone, GPP decreases are largely between 5% to 8% / 2% to 4% for the high/low
671 plant O₃ sensitivity respectively, with large areas minimally affected by O₃ damage (Figure 7), consistent with
672 lower g_s of needle leaf trees that dominate this region, and so lower O₃ uptake (Fig. S17 & S18). In the temperate
673 region, O₃ damage is extensive with reductions in GPP dominantly from 10% to 15% for the low and high plant
674 O₃ sensitivity respectively. Across significant areas of this region reductions in GPP are up to 20% under high
675 plant O₃ sensitivity (Figure 7). In the Mediterranean region, O₃ damage reduces GPP by 5% to 15% / 3% to 6%
676 for the high/low plant O₃ sensitivity respectively, with some areas seeing greater losses of up to 20% under the
677 high plant O₃ sensitivity, but this is less extensive than that seen in the temperate zone (Figure 7). In these drier
678 regions, O₃ induced stomatal closure can increase available soil moisture (Fig. S17 & S18).

679

680 The run_both_CO2+O3 simulation shows that CO₂ induced stomatal closure can help alleviate O₃ damage by
681 reducing the uptake of O₃ (Table S6). In these simulations, CO₂-induced stomatal closure was found to offset O₃-
682 suppression of GPP, such that GPP by 2050 is 3% to 7% lower due to O₃ exposure (run_both_CO2+O3), rather
683 than 4% to 9% lower in the absence of increasing CO₂ (run_O3, Table S6). Figure 6 shows this spatially, O₃
684 damage is reduced when the effect of atmospheric CO₂ on stomatal closure is accounted for, however despite this,
685 the land carbon sink and GPP remain significantly reduced due to O₃ exposure.

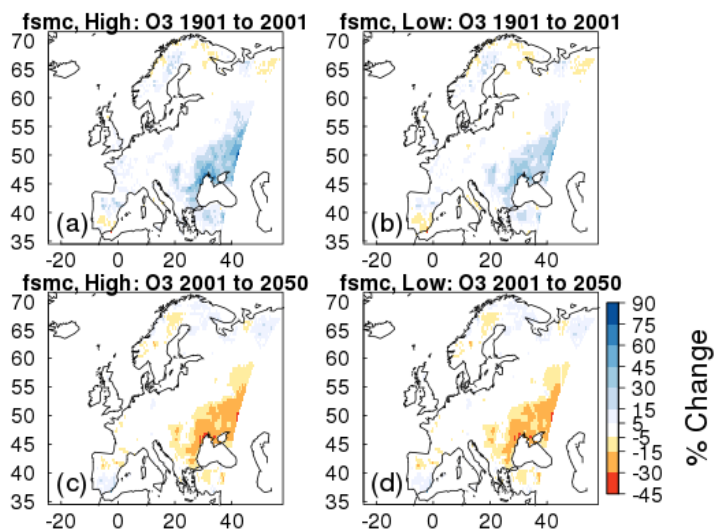
686

687 From 1901 to 2050, run_both_CO2+O3 results in an increase in European land carbon uptake (+5% to +9%), and
 688 an increase in GPP (+20% to +23%) by 2050 for the high and low plant O₃ sensitivity, respectively (Table 1).
 689 Nevertheless, despite this increase there remains a large negative impact of O₃ on the European land carbon sink
 690 (Fig. S19). By 2050 the simulated enhancement of land carbon and GPP in response to elevated CO₂ alone
 691 (run_CO2) is reduced by 3% to 6% (land carbon) and 4% to 9% (GPP) for the low and high plant O₃ sensitivity
 692 respectively, when O₃ is also accounted for (run_both_CO2+O3, Table 1). This is a large reduction in the ability
 693 of the European terrestrial biosphere to sequester carbon.
 694



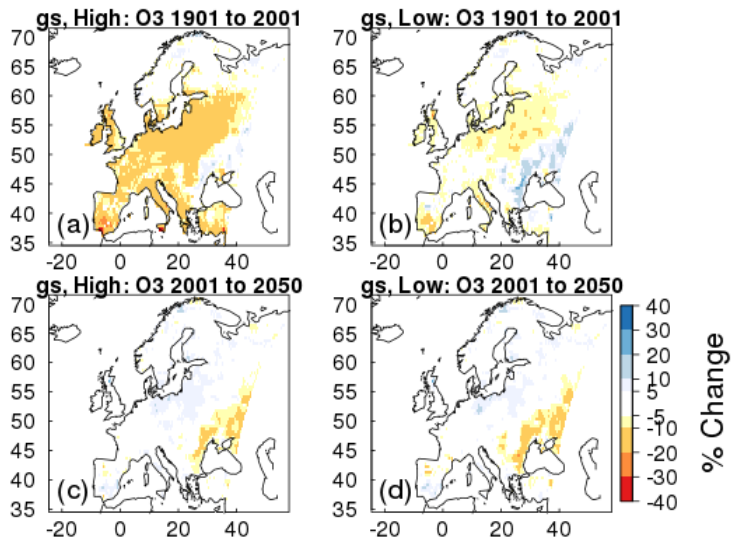
695

696 **Figure 4.** Simulated percentage change in total carbon stocks (Land C) and gross primary productivity (GPP) due
 697 to O₃ effects at fixed pre-industrial atmospheric CO₂ concentration (run_O3). Changes are shown for the periods
 698 1901 to 2001, and 2001 to 2050 for the high and low plant O₃ sensitivity.
 699

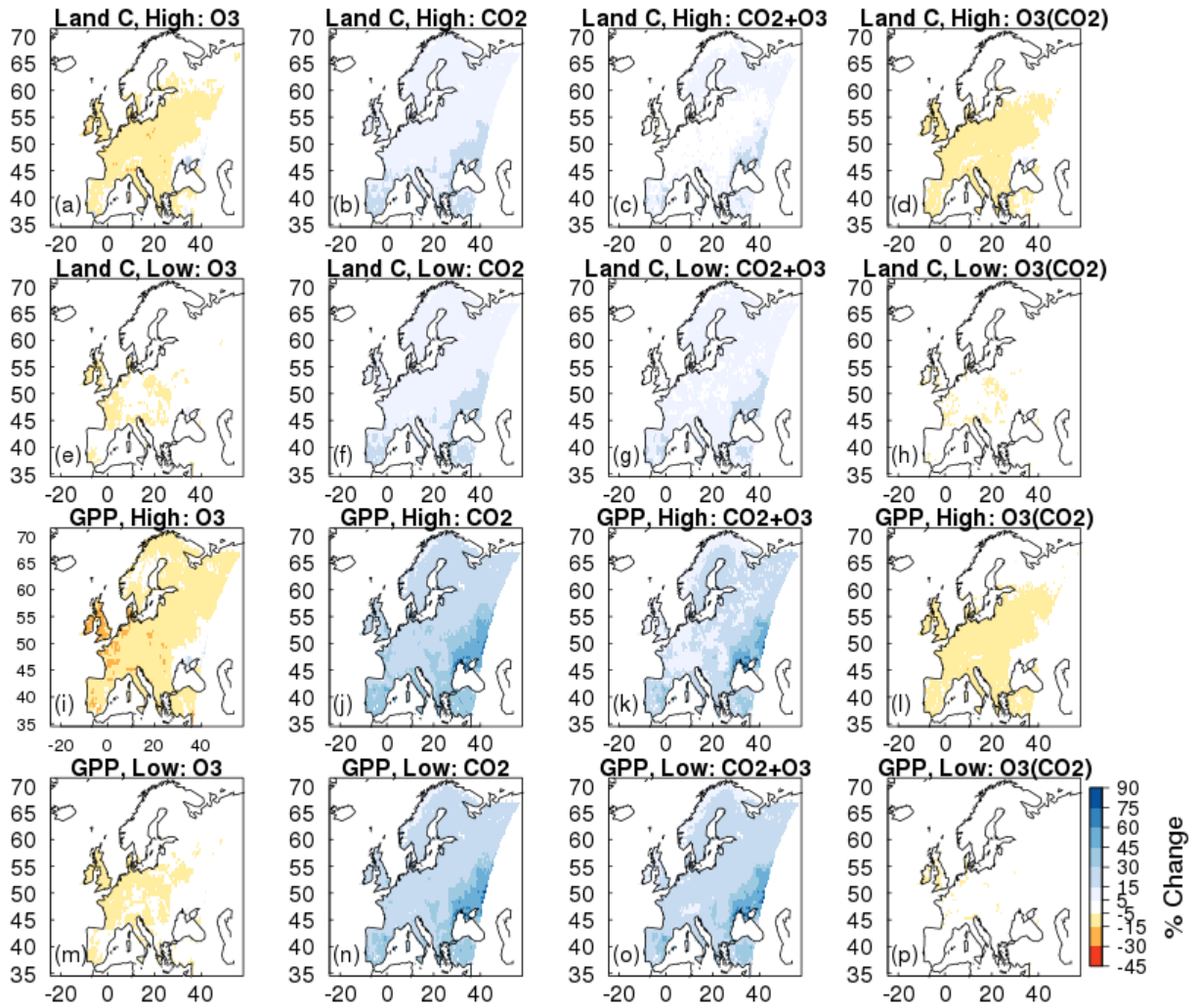


700

701 **Figure 5.** Simulated percentage change in plant available soil moisture (*fsmc*) due to O₃ effects at fixed pre-
702 industrial atmospheric CO₂ concentration (run_O3). Changes are shown for the periods 1901 to 2001, and 2001
703 to 2050 for the high and low plant O₃ sensitivity.
704



705
706 **Figure 6.** Simulated percentage change in stomatal conductance (*g_s*) due to O₃ effects at fixed pre-industrial
707 atmospheric CO₂ concentration (run_O3). Changes are shown for the periods 1901 to 2001, and 2001 to 2050 for
708 the high and low plant O₃ sensitivity.
709



710

711 **Figure 7.** Simulated percentage change in total carbon stocks (Land C) and gross primary productivity (GPP) due
 712 to i) (a, e, i, m) O₃ effects at fixed pre-industrial atmospheric CO₂ concentration (run_O3), ii) (b, f, j, n) CO₂
 713 fertilisation at fixed pre-industrial O₃ concentration (run_CO2), iii) (c, g, k, o) the interaction between O₃ and CO₂
 714 effects (run_both_CO2+O3) iv) (d, h, l, p) O₃ effects with changing atmospheric CO₂ concentration (i.e. O₃
 715 damage accounting for the effect of CO₂ induced stomatal closure; run_both_CO2+O3 – run_CO2). Changes are
 716 depicted for the periods 1901 to 2050 for high and lower ozone plant sensitivity.

717

718

719

720

721

722

723

| | High Plant O₃ Sensitivity | | | | | |
|---------------------------------------|---|------------------|---------------------------------|------------------|---------------------------------|------------------|
| | 1901 - 2001 | | 2001 - 2050 | | 1901 - 2050 | |
| | GPP (Pg C yr ⁻¹) | Land C (Pg C) | GPP (Pg C yr ⁻¹) | Land C (Pg C) | GPP (Pg C yr ⁻¹) | Land C (Pg C) |
| Value in 1901: | 9.05 | 167 | - | - | 9.05 | 167 |
| Absolute Change: | | | | | | |
| O₃ | -0.81 | -9.21 | 0.01 | -2.44 | -0.80 | -11.65 |
| CO₂ | 1.16 | 4.24 | 1.42 | 12.98 | 2.58 | 17.22 |
| CO₂ + O₃ | 0.13 | -3.28 | 1.66 | 11.11 | 1.79 | 7.83 |
| % Change: | | | | | | |
| O₃ | -8.95 | -5.51 | 0.12 | -1.55 | -8.84 | -6.98 |
| CO₂ | 12.82 | 2.54 | 13.91 | 7.58 | 28.51 | 10.31 |
| CO₂ + O₃ | 1.44 | -1.96 | 18.08 | 6.79 | 19.78 | 4.69 |
| | Low Plant O₃ Sensitivity | | | | | |
| | 1901 - 2001 | | 2001 - 2050 | | 1901 - 2050 | |
| | GPP (Pg C yr ⁻¹) | Land C (Pg C) | GPP (Pg C yr ⁻¹) | Land C (Pg C) | GPP (Pg C yr ⁻¹) | Land C (Pg C) |
| Value in 1901: | 9.34 | 167.5 | - | - | 9.34 | 167.5 |
| Absolute Change: | | | | | | |
| O₃ | -0.30 | -3.59 | 0.02 | -1.07 | -0.40 | -4.66 |
| CO₂ | 1.15 | 6.43 | 1.35 | 13.14 | 2.50 | 19.57 |
| CO₂ + O₃ | 0.65 | 2.50 | 1.50 | 12.35 | 2.15 | 14.85 |
| % Change: | | | | | | |
| O₃ | -3.21 | -2.14 | 0.22 | -0.65 | -4.28 | -2.78 |
| CO₂ | 12.31 | 3.84 | 12.87 | 7.55 | 26.77 | 11.68 |
| CO₂ + O₃ | 6.96 | 1.49 | 15.02 | 7.26 | 23.02 | 8.87 |

724

725 **Table 1.** Simulated changes in the European land carbon cycle due to changing O₃ and CO₂ concentrations
726 (independently and together). Shown are changes in total carbon stocks (Land C) and gross primary productivity
727 (GPP), over three different periods (historical: 1901 to 2001, future: 2001 to 2050, and full time series: 1901 to
728 2050). Absolute (top) and relative (bottom) differences are shown. For 2001 to 2050, please refer to Table S4 for
729 the initial value for each run. See the SI for details of the estimation of the O₃ and CO₂ effects and their interaction.

730

731

732

733

734

735

736

737

738

739

| | Mean (Pg C) | | | | |
|---|-------------|-----------|-----------|-----------|-----------|
| | 1970-1979 | 1980-1989 | 1990-1999 | 2000-2009 | 2002-2011 |
| Modelled O₃ effect on land C sink : | | | | | |
| Higher sensitivity | -1.32 | -1.01 | -0.97 | -0.53 | -0.50 |
| Low sensitivity | -0.71 | -0.58 | -0.50 | -0.29 | -0.26 |
| Sum of C emissions from fossil fuel combustion and cement production (Pg C) | | | | | |
| | 8.39 | 8.63 | 12.26 | 12.83 | 12.75 |
| C lost from O₃ effect as a % of fossil fuel and cement emissions (%): | | | | | |
| Higher sensitivity | -15.73 | -11.70 | -7.91 | -4.13 | -3.92 |
| Low sensitivity | -8.46 | -6.72 | -4.08 | -2.26 | -2.04 |

740

741 **Table 2.** Simulated change in total land carbon due to O₃ damage with changing atmospheric CO₂ concentration
742 for the two vegetation sensitivities. The sum of carbon emissions for each decade from fossil fuel combustion and
743 cement production for the EU-28 countries plus Albania, Bosnia and Herzegovina, Iceland, Belarus, Serbia,
744 Moldova, Norway, Turkey, Ukraine, Switzerland and Macedonia (EU28-plus) are shown, the data is from Boden
745 *et al.*, 2013. The simulated change in land carbon as a result of O₃ damage is depicted as a percentage of the EU28-
746 plus emissions to demonstrate the magnitude of the additional source of carbon to the atmosphere from plant O₃
747 damage.

748

749 **4 Discussion**

750

751 **4.1 Evaluation of g_s models and JULES O₃ model**

752

753 Comparison of the new g_s model implemented in this study (MED) with the g_s model currently used as standard
754 in JULES (JAC) revealed large differences in g_s for each PFT, principally as a result of the data-based
755 parameterisation of the new model. Water use increased for the broadleaf tree and C₃ herbaceous PFTs using the
756 MED model compared to JAC, but decreased for the needle leaf tree, C₄ herbaceous and shrub PFTs which
757 displayed a more conservative water use strategy compared to JAC. These changes are in line with the work of
758 De Kauwe *et al.* (2015) who found a reduction in annual transpiration for evergreen needle leaf, tundra and C₄
759 grass regions when implementing the Medlyn g_s model into the Australian land surface scheme CABLE. Site-
760 level evaluation of the models against Fluxnet observations showed that in general the MED model improved
761 simulated seasonal cycles of latent and sensible heat. The magnitude of the improvement varied with site,
762 improvements were seen at the deciduous savanna site, and at the NT sites and BT site (US_UMB) in the spring
763 and summer. However, much smaller improvements were seen at the grass sites. Changes in g_s in this study
764 resulted in differences in latent and sensible heat fluxes. Changes in the partitioning of energy fluxes at the land
765 surface could have consequences for the intensity of heatwaves (Cruz *et al.*, 2010;Kala *et al.*, 2016), runoff (Betts
766 *et al.*, 2007;Gedney *et al.*, 2006) and rainfall patterns (de Arellano *et al.*, 2012), although fully coupled simulations
767 would be necessary to detect these effects. The differences in simulated g_s led to differences in uptake of O₃
768 between the two models because the rate of g_s is the predominant determinant of the flux of O₃ through stomata.

769 Higher O₃ uptake is indicative of greater damage. Therefore, given that C₃ herbaceous vegetation is the dominant
770 land cover class across the European domain used in this study, this suggests a greater O₃ impact for Europe would
771 be simulated with MED model compared to JAC in our simulations where chemistry is uncoupled from the land
772 surface.

773

774 We evaluated the JULES O₃ model by comparing modelled GPP against the Jung et al (2011) MTE product.
775 Similar spatial patterns of GPP were simulated by JULES compared to MTE. Zonal means also showed similar
776 patterns of GPP, although JULES under predicted GPP compared to MTE at latitudes >45°N (temperate and boreal
777 regions; all simulations) and over predicted GPP at latitudes <45°N (Mediterranean region; all simulations). The
778 simulations with transient O₃ (i.e. O₃ and CO₂+O₃) showed large differences in GPP between the high and low
779 plant O₃ sensitivity simulations, this is to be expected given that the high plant O₃ sensitivity simulations were
780 parameterised to be ‘damaged’ more by O₃, i.e. greater reduction of photosynthesis/g_s with O₃ exposure compared
781 to the low plant O₃ sensitivity simulations. This difference was largest in the temperate zone, largely because of
782 C₃ grass cover being the dominant land cover here and the difference in the sensitivity to O₃ between the high and
783 low calibrations is significantly larger for C₃ grasses compared to the needle leaf trees that dominate in the boreal
784 region. Additionally, a longer growing season in the temperate region may allow for greater uptake of O₃ into
785 vegetation. C₃ grass is also the dominant land cover in the Mediterranean region with a different calibration used
786 for Mediterranean grasses for the low plant O₃ sensitivity which is less sensitive to O₃ than the temperate C₃
787 grasses, but high soil moisture stress is common throughout the growing season in the Mediterranean limiting the
788 uptake of O₃ through stomata, which likely diminishes the difference between the high and low calibrations. In
789 general, incorporating plant O₃ damage into JULES leads to worse agreement with the MTE GPP product,
790 however, this is expected to some degree as we are adding an explicit representation of O₃ damage to a model
791 calibrated to reproduce current day GPP and draw down of atmospheric CO₂. Inevitably this implicitly includes
792 O₃ damage to vegetation. Explicit representation of plant O₃ damage is important to investigate how O₃ damage
793 changes through time, under different emissions scenario’s, and the interactive effects with other gases (such as
794 CO₂) and with climate change. The percentage changes we simulate are therefore important to demonstrate the
795 sensitivity of modelled GPP and land Carbon to this process.

796

797 **4.2 Comparison of modelled estimates of O₃ damage**

798

799 Our estimates suggest O₃ (run_O₃) reduced GPP by 2001 by 3% to 9% on average across Europe and NPP by 5%
800 to 11% for the low and high plant O₃ sensitivities respectively (Table S3). Anav et al. (2011) simulated a 22%
801 reduction of GPP across Europe for 2002 using the ORCHIDEE model. Present day O₃ exposure reduced GPP by
802 10% to 25% in Europe, and 10.8% globally in the study by Lombardozzi et al. (2015) using the Community land
803 model (CLM). O₃ reduced NPP by 11.2% in Europe from 1989 to 1995 using the Terrestrial Ecosystem Model
804 (TEM) (Felzer et al., 2005). Globally, concentrations of O₃ predicted for 2100 reduced GPP by 14% to 23% using
805 a former parameterisation of O₃ sensitivity in JULES (Sitch et al., 2007). The recent study by Franz et al. (2017)
806 showed mean GPP declined by 4.7% over the period 2001 to 2010 using the OCN model over the same European

807 domain and using the same O₃ forcing produced by EMEP MSC-W as used in this study. Our estimates of changes
808 in current day GPP and NPP are at the lower end of previously modelled estimates. Simulated O₃ impacts will be
809 dependent on model O₃ concentrations, meteorology, plant sensitivity to O₃, and process representation of O₃
810 damage. It is therefore difficult to hypothesise as to exactly why modelled estimates differ, but suggests that an
811 ensemble approach to modelling O₃ impacts on the terrestrial biosphere would be beneficial to understand some
812 of these differences and provide estimates of O₃ damage with uncertainties.

813

814 **4.3 Impacts of O₃ at the land surface**

815

816 In this study, O₃ has a detrimental effect on the size of the land carbon sink for Europe. This is primarily through
817 a decrease in the size of the soil carbon pool as a result of reduced litter input to the soil, consistent with reduced
818 GPP/NPP. Field studies show that in some regions of Europe, soil carbon stocks are decreasing (Bellamy et al.,
819 2005;Capriel, 2013;Heikkinen et al., 2013;Sleutel et al., 2003). The study of Bellamy et al. (2005), for example,
820 showed that carbon was lost from soils across England and Wales between 1978 to 2003 at a mean rate of 0.6%
821 per year with little effect of land use on the rate of carbon loss, suggesting a possible link to climate change. It is
822 understood that climate change is likely to affect soil carbon turnover. Increased temperatures increase microbial
823 decomposition activity in the soil, and therefore increase carbon losses through higher rates of respiration (Cox et
824 al., 2000;Friedlingstein et al., 2006;Jones et al., 2003). However, some studies have found that O₃ can decrease
825 soil carbon content. Talhelm et al. (2014), for example, found O₃ reduced carbon content in near surface mineral
826 soil of forest soils exposed to 11 years of O₃ fumigation. Hofmocker et al. (2011) found elevated O₃ reduced the
827 carbon content in more stable soil organic matter pools, and Loya et al. (2003) showed that the fraction of soil
828 carbon formed in forest soils over a 4 year experimental period when fumigated with both CO₂ and O₃ was reduced
829 by 51% compared to the soil fumigated with CO₂ alone. It is agreed that amongst other factors that change with
830 O₃ exposure such as litter quality and composition, reduced litter quantity also has significant detrimental
831 consequences for soil carbon stocks (Andersen, 2003;Lindroth, 2010;Loya et al., 2003). Results from this study
832 therefore suggest that increasing tropospheric O₃ may be a contributing factor to the declining soil carbon stocks
833 observed across Europe as a result of reduced litter input to the soil carbon pool consistent with reduced NPP.

834

835 We acknowledge, however, that our model simulations do not include coupling of Nitrogen and Carbon cycles,
836 or land management practices. We include a representation of agricultural regions through the model calibration
837 against the wheat O₃ sensitivity function (CLRTAP, 2017), and in our simulations the high plant O₃ sensitivity
838 scenario uses this calibration against wheat for all C₃/C₄ land cover which dominates our model domain. Wheat is
839 known to be one of the most O₃ sensitive crop species however, so it is possible that our simulations over-estimate
840 the O₃ impact at the land surface. However, the low plant O₃ sensitivity calibration against natural grasslands
841 provides a counter estimate of the impact of O₃ at the land surface, therefore it is important to consider the range
842 our results provide (i.e. both the high and low plant O₃ sensitivity) as an indicator of the impact of O₃ on the land
843 surface. As with all uncoupled modelling studies, a change in g_s and flux will impact the O₃ concentration itself.
844 Therefore adopting the Medlyn formulation with a higher g_s and subsequently higher O₃ flux for broadleaf and C₃
845 PFTs (Fig 2) would lead to reduced O₃ concentration, which in turn may dampen the effect of higher g_s on O₃ flux,
846 although the higher uptake of O₃ by vegetation may lead to more damage and increase O₃ concentrations, in an

847 uncoupled chemistry-land modelling system such as this it is not possible to predict which process would
848 dominate. Additionally, this version of JULES does not have a crop module; it has no land management practices
849 such as harvesting, ploughing or crop rotation – processes which may have counteracting effects on the land
850 carbon sink. Further, without a coupled Carbon and Nitrogen cycle, it is likely that the CO₂ fertilisation response
851 of GPP and the land carbon sink is over estimated in some regions of our simulations since nitrogen availability
852 limits terrestrial carbon sequestration of natural ecosystems in the temperate and boreal zone (Zaehle, 2013). This
853 would have consequences for our modelled O₃ impact, particularly into the future where the large CO₂ fertilisation
854 effect was responsible for partly offsetting the negative impact of O₃. Although in our simulations a high fraction
855 of land cover is agricultural which we assume would be optimally fertilised. Our simulations also use a fixed
856 climate, so we do not include the effect of climate change on shifting plant phenology. Therefore, our results may
857 underestimate plant O₃ damage, since if the growing season started earlier or finished later, plants in some regions
858 would be exposed to higher O₃ concentrations. Nevertheless, we emphasise that this study provides a sensitivity
859 assessment of the impact of plant O₃ damage on GPP and the land carbon sink.

860

861 Another caveat we fully acknowledge is that at the leaf-level JULES is parameterised to reduce g_s with O₃
862 exposure. Whilst this response is commonly observed (Wittig et al., 2007; Ainsworth et al., 2012), there is evidence
863 to suggest that O₃ impairs stomata in some species, making them non-responsive to environmental stimuli (Hayes
864 et al., 2012; Hoshika et al., 2012a; Mills et al., 2009; Paoletti and Grulke, 2010). In drought conditions the
865 mechanism is thought to involve O₃ stimulated ethylene production which interferes with the stomatal response
866 to ABA signalling (Wilkinson and Davies, 2009; Wilkinson and Davies, 2010). Such stomatal sluggishness can
867 result in higher O₃ uptake and injury, increased water-loss, and therefore greater vulnerability to environmental
868 stresses (Mills et al., 2016). McLaughlin (2007a; 2007b) and Sun et al. (2012) provide evidence of increased
869 transpiration and reduced streamflow in forests at the regional scale in response to ambient levels of O₃, and
870 suggest this could increase the frequency and severity of droughts. Hoshika et al. (2012b) however found that
871 despite sluggish stomatal control in O₃ exposed trees, whole tree water use was lower in these trees because of
872 lower gas exchange and premature leaf shedding of injured leaves. To our knowledge, the study of Hoshika et al.
873 (2015) is the first to include an explicit representation of sluggish stomatal control in a land-atmosphere model,
874 they show that sluggish stomatal behaviour has implications for carbon and water cycling in ecosystems.
875 However, it is by no means a ubiquitous response, and it is not fully understood which species respond this way
876 and under what conditions (Mills et al., 2016; Wittig et al., 2007). Nevertheless, this remains an important area of
877 future work.

878

879 In this work we implement the stomatal closure proposed in Medlyn et al., (2011), this uses the parameter g_l .
880 Hoshika et al. (2013) show a significant difference in the g_l parameter (higher in elevated O₃ compared to ambient)
881 in Siebold's beech in June of their experiment. However, this is only at the start of the growing season, further
882 measurements show no difference in this parameter between O₃ treatments. Quantifying an O₃ effect directly on
883 g_l would require a detailed meta-analysis of empirical data on photosynthesis and g_s for different PFTs, which is
884 currently lacking in the literature.

885

886

887 A further caveat of this study is that the O₃ concentrations used to force the model are offline, in this case generated
888 by the EMEP MSC-W model. This means the depositional sink is different in JULES (Medlyn formulation),
889 compared to the EMEP model which uses the g_s formulation presented in Emberson et al. (2000) and Emberson
890 et al. (2001). Because we link two different model systems, the g_s values in the EMEP model differ from those
891 obtained using the Medlyn formulation, which would ultimately lead to different O₃ concentrations. The role of
892 EMEP in this study is to provide O₃ concentrations at the top of the vegetation canopy to force JULES and not g_s ,
893 how the different depositional sinks would affect simulated O₃ concentrations at canopy height has not been
894 investigated.

895

896 These offline simulations show the sensitivity of GPP and the land carbon sink to tropospheric O₃, suggesting that
897 O₃ is an important predictor of future GPP and the land carbon store across Europe. There are uncertainties in our
898 estimates however from the use of uncoupled tropospheric chemistry, meteorology and stomatal function. For
899 example, increased frequency of drought in the future would reduce stomatal conductance (assuming no sluggish
900 stomatal response) and thus O₃ uptake. Since our offline simulations do not include this feedback it is possible the
901 O₃ effect is over estimated here. Given the complexity of potential interactions and feedbacks it remains difficult
902 to diagnose the importance of individual factors (e.g. the direct physiological response) in a fully coupled
903 simulation. Once the importance of a process is demonstrated offline, it provides evidence of the need to
904 incorporate such process in coupled regional and global simulations.

905

906 **4.4 O₃ as a missing component of carbon cycle assessments?**

907

908 Comprehensive analyses of the European carbon balance suggest a large biogenic carbon sink (Janssens et al.,
909 2003;Luyssaert et al., 2012;Schulze et al., 2009). However, estimates are hampered by large uncertainties in key
910 components of the land carbon balance, such as estimates of soil carbon gains and losses (Ciais et al.,
911 2010;Janssens et al., 2003;Schulze et al., 2009;Schulze et al., 2010). We suggest that the effect of O₃ on plant
912 physiology is a contributing factor to the decline in soil carbon stores observed across Europe, and as such this O₃
913 effect is a missing component of European carbon cycle assessments. Over the full experimental period (1901 to
914 2050), our results show elevated O₃ concentrations reduce the amount of carbon that can be stored in the soil by
915 3% to 9% (low and high plant O₃ sensitivity, respectively), which almost completely offsets the beneficial effects
916 of CO₂ fertilisation on soil carbon storage under the high plant O₃ sensitivity . This would contribute to a change
917 in the size of a key carbon sink for Europe, and is particularly important when we consider the evolution of the
918 land carbon sink into the future given the impact of O₃ on soil carbon sequestration and the high uncertainty of
919 future tropospheric O₃ concentrations. Schulze et al. (2009) and Luyssaert et al. (2012) extended their analysis of
920 the European carbon balance to include additional non-CO₂ greenhouse gases (CH₄ and N₂O). Both studies found
921 that emissions of these offset the biogenic carbon sink, reducing the climate mitigation potential of European
922 ecosystems. This highlights the importance of accounting for all fluxes and stores in carbon/greenhouse gas
923 balance assessments, of which O₃ and its indirect effect on the CO₂ flux via direct effects on plant physiology is
924 currently missing.

925

926 **4.5 Interactive effects of O₃ and CO₂**

927

928 We looked at the interactive effects of CO₂ and O₃. Our results support the hypothesis that elevated atmospheric
929 CO₂ provides some protection against O₃ damage because of lower g_s that reduces uptake of O₃ through stomata
930 (Harmens et al., 2007; Wittig et al., 2007). In the present study, reductions in GPP and the land carbon store due
931 to O₃ exposure were lower when simulated with concurrent changes in atmospheric CO₂. Despite acclimation of
932 photosynthesis after long-term exposure to elevated atmospheric CO₂ of field grown plants (Ainsworth and Long,
933 2005; Medlyn et al., 1999), there is no evidence to suggest that g_s acclimates (Ainsworth et al., 2003; Medlyn et al.,
934 2001). This suggests the protective effect of elevated atmospheric CO₂ against O₃ damage will be sustained in the
935 long term. However, although meta-analysis suggest a general trend of reduced g_s with elevated CO₂ (Ainsworth
936 and Long, 2005; Medlyn et al., 1999), this is not a universal response. Stomatal responses on exposure to elevated
937 CO₂ with FACE treatment varied with genotype and growth stage in a fast-growing poplar community (Bernacchi
938 et al., 2003; Tricker et al., 2009). In other mature forest stands, limited stomatal response to elevated CO₂ was
939 observed after canopy closure (Ellsworth, 1999; Uddling et al., 2009). Also, some studies found that stomatal
940 responses to CO₂ were significant only under high atmospheric humidity (Cech et al., 2003; Leuzinger and Körner,
941 2007; Wullschlegel et al., 2002). These examples illustrate that stomatal responses to elevated atmospheric CO₂
942 are not universal, and as such the protective effect of CO₂ against O₃ injury cannot be assumed for all species, at
943 all growth stages under wide ranging environmental conditions.

944

945 **5 Conclusion**

946

947 What is abundantly clear is that plant responses to both CO₂ and O₃ are complicated by a host of factors that are
948 only partly understood, and it remains difficult to identify general, global patterns given that effects of both gases
949 on plant communities and ecological interactions are highly context and species specific (Ainsworth and Long,
950 2005; Fuhrer et al., 2016; Matyssek et al., 2010b). This study quantifies the sensitivity of the land carbon sink for
951 Europe and GPP to changing concentrations of atmospheric CO₂ and O₃ from 1901 to 2050. We have used a state
952 of the art land surface model calibrated for European vegetation to give our best estimates of this sensitivity within
953 the limits of data availability to calibrate the model for O₃ sensitivity, current knowledge and model structure. In
954 summary, this study has shown that potential gains in terrestrial carbon sequestration over Europe resulting from
955 elevated CO₂ can be partially offset by concurrent rises in tropospheric O₃ over 1901-2050. Specifically, we have
956 shown that the negative effect of O₃ on the land carbon sink was greatest over the twentieth century, when O₃
957 concentrations increased rapidly from pre-industrial levels. Over this period soil carbon stocks were diminished
958 over agricultural areas, consistent with reduced NPP and litter input. This loss of soil carbon was largely
959 responsible for the decrease in the size of the land carbon sink over Europe. The O₃ effect on the land carbon store
960 and flux was reduced into the future as CO₂ concentration rose considerably and changes in O₃ concentration were
961 less pronounced. However, there remained a large cumulative negative impact on the land carbon sink for Europe
962 by 2050. The interaction between the two gases was found to reduce O₃ injury owing to reduced stomatal opening
963 in elevated atmospheric CO₂. However, primary productivity and land carbon storage remained suppressed by
964 2050 due to plant O₃ damage. Expressed as a percentage of the emissions from fossil fuel and cement production
965 for the EU28-plus countries, the carbon emissions from O₃-induced plant injury are a source of anthropogenic
966 carbon previously not accounted for in carbon cycle assessments. Our results demonstrate the sensitivity of

967 modelled terrestrial carbon dynamics to the direct effect of tropospheric O₃ and its interaction with atmospheric
968 CO₂ on plant physiology, demonstrating this process is an important predictor of future GPP and trends in the
969 land-carbon sink. Nevertheless, this process remains largely unconsidered in regional and global climate model
970 simulations that are used to model carbon sources and sinks and carbon-climate feedbacks.

971

972

973

974 **Data availability**

975

976 The JULES model can be downloaded from the Met Office Science Repository Service
977 (<https://code.metoffice.gov.uk/trac/jules> - see here for a helpful how to [http://jules.jchmr.org/content/getting-](http://jules.jchmr.org/content/getting-started)
978 started). Model output data presented in this paper and the exact version of JULES with namelists are available
979 upon request from the corresponding author.

980

981 **Supplementary Information**

982

983 Supplementary_Information_Oliver_et_al_vn4.0.docx

984

985 **Competing Interests**

986 The authors declare that they have no conflict of interest

987

988 **Acknowledgements**

989

990 RJO and LMM were supported by the EU FP7 (ECLAIRE, 282910) and JWCRP (UKESM, NEC05816). This
991 work was also supported by EMEP under UNECE. SS and LMM acknowledge the support of the NERC
992 SAMBBA project (NE/J010057/1). The UK Met Office contribution was funded by BEIS under the Hadley Centre
993 Climate Programme (GA01101). GAF also acknowledges funding from the EU's Horizon 2020 research and
994 innovation programme (CRESCENDO, 641816). We also thank Magnuz Engardt of SMHI for providing the
995 RCA3 climate dataset. This work used eddy covariance data acquired and shared by the FLUXNET community,
996 including these networks: AmeriFlux, AfriFlux, AsiaFlux, CarboAfrica, CarboEuropeIP, CarboItaly, CarboMont,
997 ChinaFlux, Fluxnet-Canada, GreenGrass, ICOS, KoFlux, LBA, NECC, OzFlux-TERN, TCOS-Siberia, and
998 USCCC. The ERA-Interim reanalysis data are provided by ECMWF and processed by LSCE. The FLUXNET
999 eddy covariance data processing and harmonization was carried out by the European Fluxes Database Cluster,
1000 AmeriFlux Management Project, and Fluxdata project of FLUXNET, with the support of CDIAC and ICOS
1001 Ecosystem Thematic Center, and the OzFlux, ChinaFlux and AsiaFlux offices. We also thank the two anonymous
1002 reviewers who helped to improve this manuscript.

1003

1004

1005 **References**

- 1007 Ainsworth, E., and Long, S.: What have we learned from 15 years of free-air CO₂ enrichment (FACE)?
1008 A meta-analytic review of the responses of photosynthesis, canopy properties and plant production
1009 to rising CO₂, *New Phytologist*, 165, 351-372, 2005.
- 1010 Ainsworth, E. A., Davey, P. A., Hymus, G. J., Osborne, C. P., Rogers, A., Blum, H., Nosberger, J., and
1011 Long, S. P.: Is stimulation of leaf photosynthesis by elevated carbon dioxide concentration
1012 maintained in the long term? A test with *Lolium perenne* grown for 10 years at two nitrogen
1013 fertilization levels under Free Air CO₂ Enrichment (FACE), *Plant, Cell and Environment*, 26, 705-714,
1014 2003.
- 1015 Ainsworth, E. A.: Rice production in a changing climate: a meta-analysis of responses to elevated
1016 carbon dioxide and elevated ozone concentration, *Global Change Biology*, 14, 1642-1650,
1017 10.1111/j.1365-2486.2008.01594.x, 2008.
- 1018 Ainsworth, E. A., Yendrek, C. R., Sitch, S., Collins, W. J., and Emberson, L. D.: The Effects of
1019 Tropospheric Ozone on Net Primary Productivity and Implications for Climate Change, *Annual*
1020 *Review of Plant Biology*, 63, 637-661, doi:10.1146/annurev-arplant-042110-103829, 2012.
- 1021 Anav, A., Menut, L., Khvorostyanov, D., and Viovy, N.: Impact of tropospheric ozone on the Euro-
1022 Mediterranean vegetation, *Global change biology*, 17, 2342-2359, 2011.
- 1023 Andersen, C. P.: Source–sink balance and carbon allocation below ground in plants exposed to
1024 ozone, *New Phytologist*, 157, 213-228, 10.1046/j.1469-8137.2003.00674.x, 2003.
- 1025 Arneth, A., Harrison, S. P., Zaehle, S., Tsigaridis, K., Menon, S., Bartlein, P. J., Feichter, J., Korhola, A.,
1026 Kulmala, M., O'Donnell, D., Schurgers, G., Sorvari, S., and Vesala, T.: Terrestrial biogeochemical
1027 feedbacks in the climate system, *Nature Geosci*, 3, 525-532,
1028 http://www.nature.com/ngeo/journal/v3/n8/supinfo/ngeo905_S1.html, 2010.
- 1029 Auvray, M., and Bey, I.: Long-range transport to Europe: Seasonal variations and implications for the
1030 European ozone budget, *Journal of Geophysical Research: Atmospheres*, 110,
1031 doi:10.1029/2004JD005503, 2005.
- 1032 Avnery, S., Mauzerall, D. L., Liu, J., and Horowitz, L. W.: Global crop yield reductions due to surface
1033 ozone exposure: 1. Year 2000 crop production losses and economic damage, *Atmospheric*
1034 *Environment*, 45, 2284-2296, <https://doi.org/10.1016/j.atmosenv.2010.11.045>, 2011.
- 1035 Baig, S., Medlyn, B. E., Mercado, L. M., and Zaehle, S.: Does the growth response of woody plants to
1036 elevated CO₂ increase with temperature? A model-oriented meta-analysis, *Global Change Biology*,
1037 21, 4303-4319, 10.1111/gcb.12962, 2015.
- 1038 Bellamy, P. H., Loveland, P. J., Bradley, R. I., Lark, R. M., and Kirk, G. J.: Carbon losses from all soils
1039 across England and Wales 1978–2003, *Nature*, 437, 245-248, 2005.
- 1040 Bernacchi, C. J., Calfapietra, C., Davey, P. A., Wittig, V. E., Scarascia-Mugnozza, G. E., Raines, C. A.,
1041 and Long, S. P.: Photosynthesis and stomatal conductance responses of poplars to free-air CO₂
1042 enrichment (PopFACE) during the first growth cycle and immediately following coppice., *New*
1043 *Phytologist*, 159, 609-621, 2003.
- 1044 Best, M. J., Pryor, M., Clark, D. B., Rooney, G. G., Essery, R. L. H., Menard, C. B., Edwards, J. M.,
1045 Hendry, M. A., Porson, N., Gedney, N., Mercado, L. M., Sitch, S., Blyth, E., Boucher, O., Cox, P. M.,
1046 Grimmond, C. S. B., and Harding, R. J.: The Joint UK Land Environment Simulator (JULES), Model
1047 description - Part 1: Energy and water fluxes, *Geoscientific Model Development Discussions*, 4, 595-
1048 640, 10.5194/GMDD-4-595-2011, 2011.
- 1049 Betts, R. A., Boucher, O., Collins, M., Cox, P. M., Falloon, P. D., Gedney, N., Hemming, D. L.,
1050 Huntingford, C., Jones, C. D., and Sexton, D. M.: Projected increase in continental runoff due to plant
1051 responses to increasing carbon dioxide, *Nature*, 448, 1037-1041, 2007.
- 1052 Boden, T. A., Marland, G., and Andres, R. J.: Global, Regional, and National Fossil-Fuel CO₂ Emissions,
1053 Oak Ridge National Laboratory, U.S. Department of Energy, Oak Ridge, Tenn., USA, 2013.
- 1054 Büker, P., Feng, Z., Uddling, J., Briolat, A., Alonso, R., Braun, S., Elvira, S., Gerosa, G., Karlsson, P. E.,
1055 Le Thiec, D., Marzuoli, R., Mills, G., Oksanen, E., Wieser, G., Wilkinson, M., and Emberson, L. D.: New

1056 flux based dose-response relationships for ozone for European forest tree species, *Environmental*
1057 *Pollution*, 163-174, 2015.

1058 Calvete-Sogo, H., Elvira, S., Sanz, J., González-Fernández, I., García-Gómez, H., Sánchez-Martín, L.,
1059 Alonso, R., and Bermejo-Bermejo, V.: Current ozone levels threaten gross primary production and
1060 yield of Mediterranean annual pastures and nitrogen modulates the response, *Atmospheric*
1061 *Environment*, 95, 197-206, <http://dx.doi.org/10.1016/j.atmosenv.2014.05.073>, 2014.

1062 Capriel, P.: Trends in organic carbon and nitrogen contents in agricultural soils in Bavaria (south
1063 Germany) between 1986 and 2007, *European Journal of Soil Science*, 64, 445-454, 2013.

1064 Cech, P. G., Pepin, S., and Korner, C.: Elevated CO₂ reduces sap flux in mature deciduous forest trees,
1065 *Oecologia*, 137, 258-268, 2003.

1066 Ceulemans, R., and Mousseau, M.: Effects of elevated atmospheric CO₂ on woody plants, *New*
1067 *Phytologist*, 127, 1994.

1068 Ciais, P., Wattenbach, M., Vuichard, N., Smith, P., Piao, S., Don, A., Luysaert, S., Janssens, I.,
1069 Bondeau, A., and Dechow, R.: The European carbon balance. Part 2: croplands, *Global Change*
1070 *Biology*, 16, 1409-1428, 2010.

1071 Ciais, P., Sabine, C., Bala, G., Bopp, L., Brovkin, V., Canadell, J., Chhabra, A., DeFries, R., Galloway, J.,
1072 Heimann, M., Jones, C., Le Quéré, C., Myneni, R. B., Piao, S., and Thornton, P.: Carbon and Other
1073 Biogeochemical Cycles. In: *Climate Change 2013: The Physical Science Basis. Contribution of Working*
1074 *Group I to the Fifth Assessment Report of the Intergovernmental Panel on Climate Change* [Stocker,
1075 T.F., D. Qin, G.-K. Plattner, M. Tignor, S.K. Allen, J. Boschung, A. Nauels, Y. Xia, V. Bex and P.M.
1076 Midgley (eds.)]. Cambridge University Press, Cambridge, United Kingdom and New York, NY, USA.,
1077 2013.

1078 Clark, D. B., Mercado, L. M., Sitch, S., Jones, C. D., Gedney, N., Best, M. J., Pryor, M., Rooney, G. G.,
1079 Essery, R. L. H., Blyth, E., Boucher, O., Harding, R. J., and Cox, P. M.: The Joint UK Land Environment
1080 Simulator (JULES), Model description - Part 2: Carbon fluxes and vegetation, *Geoscientific Model*
1081 *Development Discussions*, 4, 641-688, 10.5194/gmdd-4-641-2011, 2011.

1082 CLRTAP: The UNECE Convention on Long-range Transboundary Air Pollution. Manual on
1083 Methodologies and Criteria for Modelling and Mapping Critical Loads and Levels and Air Pollution
1084 Effects, Risks and Trends: Chapter III Mapping Critical Levels for Vegetation, accessed via,
1085 [http://icpvegetation.ceh.ac.uk/publications/documents/Chapter3-](http://icpvegetation.ceh.ac.uk/publications/documents/Chapter3-Mappingcriticallevelsforvegetation_000.pdf)
1086 [Mappingcriticallevelsforvegetation_000.pdf](http://icpvegetation.ceh.ac.uk/publications/documents/Chapter3-Mappingcriticallevelsforvegetation_000.pdf), 2017.

1087 Collins, W. J., Sitch, S., and Boucher, O.: How vegetation impacts affect climate metrics for ozone
1088 precursors, *Journal of Geophysical Research: Atmospheres*, 115, D23308, 10.1029/2010JD014187,
1089 2010.

1090 Collins, W. J., Bellouin, N., Doutriaux-Boucher, M., Gedney, N., Halloran, P., Hinton, T., Hughes, J.,
1091 Jones, C. D., Joshi, M., Liddicoat, S., Martin, G., O'Connor, F., Rae, J., Senior, C., Sitch, S., Totterdell, I.,
1092 Wiltshire, A., and Woodward, S.: Development and evaluation of an Earth-System model –
1093 HadGEM2, *Geosci. Model Dev.*, 4, 1051-1075, 10.5194/gmd-4-1051-2011, 2011.

1094 Cooper, O. R., Parrish, D. D., Stohl, A., Trainer, M., Nedelec, P., Thouret, V., Cammas, J. P., Oltmans,
1095 S. J., Johnson, B. J., Tarasick, D., Leblanc, T., McDermid, I. S., Jaffe, D., Gao, R., Stith, J., Ryerson, T.,
1096 Aikin, K., Campos, T., Weinheimer, A., and Avery, M. A.: Increasing springtime ozone mixing ratios in
1097 the free troposphere over western North America, *Nature*, 463, 344-348,
1098 http://www.nature.com/nature/journal/v463/n7279/supinfo/nature08708_S1.html, 2010.

1099 Cooper, O. R., Parrish, D., Ziemke, J., Balashov, N., Cupeiro, M., Galbally, I., Gilge, S., Horowitz, L.,
1100 Jensen, N., and Lamarque, J.-F.: Global distribution and trends of tropospheric ozone: An
1101 observation-based review, *Elementa: Science of the Anthropocene*, 2, 000029, 2014.

1102 Cox, P. M., Betts, R. A., Jones, C. D., Spall, S. A., and Totterdell, I. J.: Acceleration of global warming
1103 due to carbon-cycle feedbacks in a coupled climate model, *Nature*, 408, 184-187, 2000.

1104 Cox, P. M.: Description of the TRIFFID dynamic global vegetation model, Hadley Centre technical
1105 note 24, 2001.

1106 Cruz, F. T., Pitman, A. J., and Wang, Y. P.: Can the stomatal response to higher atmospheric carbon
1107 dioxide explain the unusual temperatures during the 2002 Murray-Darling Basin drought?, *Journal of*
1108 *Geophysical Research: Atmospheres*, 115, 2010.

1109 de Arellano, J. V.-G., van Heerwaarden, C. C., and Lelieveld, J.: Modelled suppression of boundary-
1110 layer clouds by plants in a CO₂-rich atmosphere, *Nature geoscience*, 5, 701-704, 2012.

1111 De Kauwe, M., Kala, J., Lin, Y.-S., Pitman, A., Medlyn, B., Duursma, R., Abramowitz, G., Wang, Y.-P.,
1112 and Miralles, D.: A test of an optimal stomatal conductance scheme within the CABLE land surface
1113 model, 8, 431-452, 2015.

1114 Derwent, R. G., Stevenson, D. S., Doherty, R. M., Collins, W. J., Sanderson, M. G., and Johnson, C. E.:
1115 Radiative forcing from surface NO_x emissions: spatial and seasonal variations, *Climatic Change*, 88,
1116 385-401, 10.1007/s10584-007-9383-8, 2008.

1117 Derwent, R. G., Utembe, S. R., Jenkin, M. E., and Shallcross, D. E.: Tropospheric ozone production
1118 regions and the intercontinental origins of surface ozone over Europe, *Atmospheric Environment*,
1119 112, 216-224, <https://doi.org/10.1016/j.atmosenv.2015.04.049>, 2015.

1120 Ellsworth, D. S.: CO₂ enrichment in a maturing pine forest: are CO₂ exchange and water status in the
1121 canopy affected?, *Plant, Cell and Environment*, 22, 461-472, 1999.

1122 Emberson, L. D., Ashmore, M. R., Cambridge, H. M., Simpson, D., and Tuovinen, J.-P.: Modelling
1123 stomatal ozone flux across Europe, *Environmental Pollution*, 109, 403–413, 2000.

1124 Emberson, L. D., Simpson, D., Tuovinen, J.-P., Ashmore, M. R., and Cambridge, H. M.: Modelling and
1125 mapping ozone deposition in Europe, *Water Air Soil Pollution*, 130, 577–582, 2001.

1126 Emberson, L. D., Büker, P., and Ashmore, M. R.: Assessing the risk caused by ground level ozone to
1127 European forest trees: A case study in pine, beech and oak across different climate regions,
1128 *Environmental Pollution*, 147, 454–466, 2007.

1129 Engardt, M., Simpson, D., Schwikowski, M., and Granat, L.: Deposition of sulphur and nitrogen in
1130 Europe 1900-2050. Model calculations and comparison to historical observations, *Tellus B: Chem.*
1131 *Phys. Meteor.*, 69, 2017.

1132 Etheridge, D. M., Steele, L. P., Langenfelds, R. L., Francey, R. J., M., B., and Morgan, V. I.: Natural and
1133 anthropogenic changes in atmospheric CO₂ over the last 1000 years from air in Antarctic ice and firn,
1134 *Journal of Geophysical Research*, 101(D2), 4115–4128, doi:10.1029/95JD03410, 1996.

1135 Fagnano, M., Maggio, A., and Fumagalli, I.: Crops' responses to ozone in Mediterranean
1136 environments, *Environmental Pollution*, 157, 1438-1444, 2009.

1137 Fares, S., Vargas, R., Detto, M., Goldstein, A. H., Karlik, J., Paoletti, E., and Vitale, M.: Tropospheric
1138 ozone reduces carbon assimilation in trees: estimates from analysis of continuous flux
1139 measurements, *Global change biology*, 19, 2427-2443, 2013.

1140 Felzer, B., Reilly, J., Melillo, J., Kicklighter, D., Sarofim, M., Wang, C., Prinn, R., and Zhuang, Q.: Future
1141 Effects of Ozone on Carbon Sequestration and Climate Change Policy Using a Global Biogeochemical
1142 Model, *Climatic Change*, 73, 345-373, 10.1007/s10584-005-6776-4, 2005.

1143 Felzer, B. S. F., Kicklighter, D. W., Melillo, J. M., Wang, C., Zhuang, Q., and Prinn, R. G.: Ozone effects
1144 on net primary productivity and carbon sequestration in the conterminous United States using a
1145 biogeochemistry model, *Tellus*, 56B, 230-248, 2004.

1146 Feng, Z., Kobayashi, K., and Ainsworth, E. A.: Impact of elevated ozone concentration on growth,
1147 physiology, and yield of wheat (*Triticum aestivum* L.): a meta-analysis, *Global Change Biology*, 14,
1148 2696-2708, 10.1111/j.1365-2486.2008.01673.x, 2008.

1149 Fowler, D., Flechard, C., Cape, J. N., Storeton-West, R. L., and Coyle, M.: Measurements of Ozone
1150 Deposition to Vegetation Quantifying the Flux, the Stomatal and Non-Stomatal Components, *Water,*
1151 *Air, and Soil Pollution*, 130, 63-74, 10.1023/a:1012243317471, 2001.

1152 Fowler, D., Pilegaard, K., Sutton, M., Ambus, P., Raivonen, M., Duyzer, J., Simpson, D., Fagerli, H.,
1153 Fuzzi, S., and Schjørring, J. K.: Atmospheric composition change: ecosystems–atmosphere
1154 interactions, *Atmospheric Environment*, 43, 5193-5267, 2009.

1155 Franz, M., Simpson, D., Arneeth, A., and Zaehle, S.: Development and evaluation of an ozone
1156 deposition scheme for coupling to a terrestrial biosphere model, *Biogeosciences*, 14, 45-71,
1157 doi:10.5194/bg-14-45-2017, 2017.

1158 Friedlingstein, P., Cox, P., Betts, R., Bopp, L., von Bloh, W., Brovkin, V., Cadule, P., Doney, S., Eby, M.,
1159 Fung, I., Bala, G., John, J., Jones, C., Joos, F., Kato, T., Kawamiya, M., Knorr, W., Lindsay, K.,
1160 Matthews, H. D., Raddatz, T., Rayner, P., Reick, C., Roeckner, E., Schnitzler, K. G., Schnur, R.,
1161 Strassmann, K., Weaver, A. J., Yoshikawa, C., and Zeng, N.: Climate–Carbon Cycle Feedback Analysis:
1162 Results from the C4MIP Model Intercomparison, *Journal of Climate*, 19, 3337-3353,
1163 10.1175/jcli3800.1, 2006.

1164 Fuhrer, J., Val Martin, M., Mills, G., Heald, C. L., Harmens, H., Hayes, F., Sharps, K., Bender, J., and
1165 Ashmore, M. R.: Current and future ozone risks to global terrestrial biodiversity and ecosystem
1166 processes, *Ecology and Evolution*, 6, 8785-8799, 10.1002/ece3.2568, 2016.

1167 Gedney, N., Cox, P. M., Bett, R. A., Boucher, O., Huntingford, C., and Stott, P. A.: Detection of a direct
1168 carbon dioxide effect in continental river runoff records, *Nature*, 439, 835-838, 2006.

1169 Gerosa, G., Marzuoli, R., Monteleone, B., Chiesa, M., and Finco, A.: Vertical Ozone Gradients above
1170 Forests. Comparison of Different Calculation Options with Direct Ozone Measurements above a
1171 Mature Forest and Consequences for Ozone Risk Assessment, *Forests*, 8, 337, 2017.

1172 Grantz, D., Gunn, S., and VU, H. B.: O₃ impacts on plant development: a meta-analysis of root/shoot
1173 allocation and growth, *Plant, cell & environment*, 29, 1193-1209, 2006.

1174 Harmens, H., Mills, G., Emberson, L. D., and Ashmore, M. R.: Implications of climate change for the
1175 stomatal flux of ozone: A case study for winter wheat, *Environmental Pollution*, 146, 763-770,
1176 <http://dx.doi.org/10.1016/j.envpol.2006.05.018>, 2007.

1177 Hayes, F., Wagg, S., Mills, G., Wilkinson, S., and Davies, W.: Ozone effects in a drier climate:
1178 implications for stomatal fluxes of reduced stomatal sensitivity to soil drying in a typical grassland
1179 species, *Global Change Biology*, 18, 948-959, 2012.

1180 Heikkinen, J., Ketoja, E., Nuutinen, V., and Regina, K.: Declining trend of carbon in Finnish cropland
1181 soils in 1974–2009, *Global Change Biology*, 19, 1456-1469, 10.1111/gcb.12137, 2013.

1182 Hofmockel, K. S., Zak, D. R., Moran, K. K., and Jastrow, J. D.: Changes in forest soil organic matter
1183 pools after a decade of elevated CO₂ and O₃, *Soil Biology and Biochemistry*, 43, 1518-1527,
1184 <http://dx.doi.org/10.1016/j.soilbio.2011.03.030>, 2011.

1185 Hoshika, Y., Watanabe, M., Inada, N., and Koike, T.: Ozone-induced stomatal sluggishness develops
1186 progressively in Siebold's beech (*Fagus crenata*), *Environmental Pollution*, 166, 152-156, 2012a.

1187 Hoshika, Y., Omasa, K., and Paoletti, E.: Whole-Tree Water Use Efficiency Is Decreased by Ambient
1188 Ozone and Not Affected by O₃-Induced Stomatal Sluggishness, *PLOS ONE*, 7, e39270,
1189 10.1371/journal.pone.0039270, 2012b.

1190 Hoshika, Y., Watanabe, M., Inada, N., and Koike, T.: Model-based analysis of avoidance of ozone
1191 stress by stomatal closure in Siebold's beech (*Fagus crenata*), *Annals of Botany*, 112, 1149-1158,
1192 2013.

1193 Hoshika, Y., Katata, G., Deushi, M., Watanabe, M., Koike, T., and Paoletti, E.: Ozone-induced stomatal
1194 sluggishness changes carbon and water balance of temperate deciduous forests., *Scientific Reports*,
1195 doi:10.1038/srep09871, 2015.

1196 Hurtt, G., Chini, L. P., Frolking, S., Betts, R., Feddema, J., Fischer, G., Fisk, J., Hibbard, K., Houghton,
1197 R., Janetos, A., and Jones, C. D.: Harmonization of land-use scenarios for the period 1500–2100: 600
1198 years of global gridded annual land-use transitions, wood harvest, and resulting secondary lands,
1199 *Climatic Change*, 109, 117-161, 2011.

1200 IGBP-DIS: International Geosphere-Biosphere Programme, Data and Information System, Potsdam,
1201 Germany. Available from Oak Ridge National Laboratory Distributed Active Archive Center, Oak
1202 Ridge, TN, available at: <http://www.daac.ornl.gov>,

1203 IPCC: Climate change 2013: The Physical Science Basis, IPCC Working Group I Contribution to AR5,
1204 2013.

1205 Jacobs, C. M. J.: Direct impact of atmospheric CO₂ enrichment on regional transpiration, Wageningen
1206 Agricultural University, 1994.

1207 Janssens, I. A., Freibauer, A., Ciais, P., Smith, P., Nabuurs, G.-J., Folberth, G., Schlamadinger, B.,
1208 Hutjes, R. W. A., Ceulemans, R., Schulze, E.-D., Valentini, R., and Dolman, A. J.: Europe's Terrestrial
1209 Biosphere Absorbs 7 to 12% of European Anthropogenic CO₂ Emissions, *Science*, 300, 1538-1542,
1210 10.1126/science.1083592, 2003.

1211 Jones, C. D., Cox, P., and Huntingford, C.: Uncertainty in climate–carbon-cycle projections associated
1212 with the sensitivity of soil respiration to temperature, *Tellus B*, 55, 642-648, 10.1034/j.1600-
1213 0889.2003.01440.x, 2003.

1214 Jung, M., Reichstein, M., Margolis, H. A., Cescatti, A., Richardson, A. D., Arain, M. A., Arneth, A.,
1215 Bernhofer, C., Bonal, D., Chen, J., Gianelle, D., Gobron, N., Kiely, G., Kutsch, W., Lasslop, G., Law, B.
1216 E., Lindroth, A., Merbold, L., Montagnani, L., Moors, E. J., Papale, D., Sottocornola, M., Vaccari, F.,
1217 and Williams, C.: Global patterns of land-atmosphere fluxes of carbon dioxide, latent heat, and
1218 sensible heat derived from eddy covariance, satellite, and meteorological observations, *Journal of*
1219 *Geophysical Research: Biogeosciences*, 116, n/a-n/a, 10.1029/2010JG001566, 2011.

1220 Kala, J., De Kauwe, M. G., Pitman, A. J., Medlyn, B. E., Wang, Y. P., Lorenz, R., and Perkins-Kirkpatrick,
1221 S. E.: Impact of the representation of stomatal conductance on model projections of heatwave
1222 intensity., *Scientific Reports*, 1-7, 10.1038/srep23418, 2016.

1223 Karlsson, P. E., Braun, S., Broadmeadow, M., Elvira, S., Emberson, L., Gimeno, B. S., Le Thiec, D.,
1224 Novak, K., Oksanen, E., Schaub, M., Uddling, J., and Wilkinson, M.: Risk assessments for forest trees:
1225 The performance of the ozone flux versus the AOT concepts, *Environmental Pollution*, 146, 608-616,
1226 <http://dx.doi.org/10.1016/j.envpol.2006.06.012>, 2007.

1227 Karnosky, D., Percy, K. E., Xiang, B., Callan, B., Noormets, A., Mankovska, B., Hopkin, A., Sober, J.,
1228 Jones, W., and Dickson, R.: Interacting elevated CO₂ and tropospheric O₃ predisposes aspen
1229 (*Populus tremuloides* Michx.) to infection by rust (*Melampsora medusae* f. sp. *tremuloidae*), *Global*
1230 *Change Biology*, 8, 329-338, 2002.

1231 Karnosky, D. F., Skelly, J. M., Percy, K. E., and Chappelka, A. H.: Perspectives regarding 50years of
1232 research on effects of tropospheric ozone air pollution on US forests, *Environmental Pollution*, 147,
1233 489-506, 2007.

1234 Keeling, C. D., and Whorf, T. P.: Atmospheric CO₂ records from sites in the SIO air sampling network.
1235 In *Trends: A Compendium of Data on Global Change*, Carbon Dioxide Information Analysis Center,
1236 Oak Ridge National Laboratory, Oak Ridge, Tenn., U.S.A. , 2004.

1237 Kitao, M., Löw, M., Heerd, C., Grams, T. E., Häberle, K.-H., and Matyssek, R.: Effects of chronic
1238 elevated ozone exposure on gas exchange responses of adult beech trees (*Fagus sylvatica*) as related
1239 to the within-canopy light gradient, *Environmental Pollution*, 157, 537-544, 2009.

1240 Kjellström, E., Nikulin, G., Hansson, U., Strandberg, G., and Ullerstig, A.: 21st century changes in the
1241 European climate: uncertainties derived from an ensemble of regional climate model simulations,
1242 *Tellus A*, 63, 24-40, 2011.

1243 Kubiske, M., Quinn, V., Marquardt, P., and Karnosky, D.: Effects of Elevated Atmospheric CO₂ and/or
1244 O₃ on Intra-and Interspecific Competitive Ability of Aspen, *Plant biology*, 9, 342-355, 2007.

1245 Lamarque, J., Shindell, D. T., Josse, B., Young, P., Cionni, I., Eyring, V., Bergmann, D., Cameron-Smith,
1246 P., Collins, W. J., and Doherty, R.: The Atmospheric Chemistry and Climate Model Intercomparison
1247 Project (ACCMIP): overview and description of models, simulations and climate diagnostics,
1248 *Geoscientific Model Development*, 6, 179-206, 2013.

1249 Langner, J., Engardt, M., Baklanov, A., Christensen, J. H., Gauss, M., Geels, C., Hedegaard, G. B.,
1250 Nuterman, R., Simpson, D., and Soares, J.: A multi-model study of impacts of climate change on
1251 surface ozone in Europe, *Atmospheric Chemistry and Physics*, 12, 10423-10440, 2012a.

1252 Langner, J., Engardt, M., and Andersson, C.: European summer surface ozone 1990–2100,
1253 *Atmospheric Chemistry and Physics*, 12, 10097-10105, 2012b.

1254 Le Quéré, C., Moriarty, R., Andrew, R. M., Peters, G. P., Ciais, P., Friedlingstein, P., Jones, S. D., Sitch,
1255 S., Tans, P., Arneth, A., Boden, T. A., Bopp, L., Bozec, Y., Canadell, J. G., Chini, L. P., Chevallier, F.,

1256 Cosca, C. E., Harris, I., Hoppema, M., Houghton, R. A., House, J. I., Jain, A. K., Johannessen, T., Kato,
1257 E., Keeling, R. F., Kitidis, V., Klein Goldewijk, K., Koven, C., Landa, C. S., Landschützer, P., Lenton, A.,
1258 Lima, I. D., Marland, G., Mathis, J. T., Metzl, N., Nojiri, Y., Olsen, A., Ono, T., Peng, S., Peters, W., Pfeil,
1259 B., Poulter, B., Raupach, M. R., Regnier, P., Rödenbeck, C., Saito, S., Salisbury, J. E., Schuster, U.,
1260 Schwinger, J., Séférian, R., Segschneider, J., Steinhoff, T., Stocker, B. D., Sutton, A. J., Takahashi, T.,
1261 Tilbrook, B., van der Werf, G. R., Viovy, N., Wang, Y. P., Wanninkhof, R., Wiltshire, A., and Zeng, N.:
1262 Global carbon budget 2014, *Earth Syst. Sci. Data*, 7, 47-85, 10.5194/essd-7-47-2015, 2015.

1263 Le Quéré, C., Andrew, R. M., Canadell, J. G., Sitch, S., Korsbakken, J. I., Peters, G. P., Manning, A. C.,
1264 Boden, T. A., Tans, P. P., Houghton, R. A., Keeling, R. F., Alin, S., Andrews, O. D., Anthoni, P., Barbero,
1265 L., Bopp, L., Chevallier, F., Chini, L. P., Ciais, P., Currie, K., Delire, C., Doney, S. C., Friedlingstein, P.,
1266 Gkritzalis, T., Harris, I., Hauck, J., Haverd, V., Hoppema, M., Klein Goldewijk, K., Jain, A. K., Kato, E.,
1267 Körtzinger, A., Landschützer, P., Lefèvre, N., Lenton, A., Lienert, S., Lombardozi, D., Melton, J. R.,
1268 Metzl, N., Millero, F., Monteiro, P. M. S., Munro, D. R., Nabel, J. E. M. S., Nakaoka, S. I., O'Brien, K.,
1269 Olsen, A., Omar, A. M., Ono, T., Pierrot, D., Poulter, B., Rödenbeck, C., Salisbury, J., Schuster, U.,
1270 Schwinger, J., Séférian, R., Skjelvan, I., Stocker, B. D., Sutton, A. J., Takahashi, T., Tian, H., Tilbrook, B.,
1271 van der Laan-Luijckx, I. T., van der Werf, G. R., Viovy, N., Walker, A. P., Wiltshire, A. J., and Zaehle, S.:
1272 Global Carbon Budget 2016, *Earth Syst. Sci. Data*, 8, 605-649, 10.5194/essd-8-605-2016, 2016.

1273 Le Quéré, C., Andrew, R. M., Friedlingstein, P., Sitch, S., Pongratz, J., Manning, A. C., Korsbakken, J. I.,
1274 Peters, G. P., Canadell, J. G., Jackson, R. B., Boden, T. A., Tans, P. P., Andrews, O. D., Arora, V. K.,
1275 Bakker, D. C. E., Barbero, L., Becker, M., Betts, R. A., Bopp, L., Chevallier, F., Chini, L. P., Ciais, P.,
1276 Cosca, C. E., Cross, J., Currie, K., Gasser, T., Harris, I., Hauck, J., Haverd, V., Houghton, R. A., Hunt, C.
1277 W., Hurtt, G., Ilyina, T., Jain, A. K., Kato, E., Kautz, M., Keeling, R. F., Klein Goldewijk, K., Körtzinger,
1278 A., Landschützer, P., Lefèvre, N., Lenton, A., Lienert, S., Lima, I., Lombardozi, D., Metzl, N., Millero,
1279 F., Monteiro, P. M. S., Munro, D. R., Nabel, J. E. M. S., Nakaoka, S.-I., Nojiri, Y., Padín, X. A., Pregon,
1280 A., Pfeil, B., Pierrot, D., Poulter, B., Rehder, G., Reimer, J., Rödenbeck, C., Schwinger, J., Séférian, R.,
1281 Skjelvan, I., Stocker, B. D., Tian, H., Tilbrook, B., van der Laan-Luijckx, I. T., van der Werf, G. R., van
1282 Heuven, S., Viovy, N., Vuichard, N., Walker, A. P., Watson, A. J., Wiltshire, A. J., Zaehle, S., and Zhu,
1283 D.: Global Carbon Budget 2017, *Earth Syst. Sci. Data Discuss*, in review, 2017.

1284 Leuzinger, S., and Körner, C.: Water savings in mature deciduous forest trees under elevated CO₂,
1285 *Global Change Biology*, 13, 2498-2508, doi:10.1111/j.1365-2486.2007.01467.x, 2007.

1286 Lin, Y.-S., Medlyn, B. E., Duursma, R. A., Prentice, I. C., Wang, H., Baig, S., Eamus, D., de Dios, V. R.,
1287 Mitchell, P., and Ellsworth, D. S.: Optimal stomatal behaviour around the world, *Nature Climate*
1288 *Change*, 5, 459-464, 2015.

1289 Lindroth, R. L.: Impacts of Elevated Atmospheric CO₂ and O₃ on Forests: Phytochemistry, Trophic
1290 Interactions, and Ecosystem Dynamics, *Journal of Chemical Ecology*, 36, 2-21, 10.1007/s10886-009-
1291 9731-4, 2010.

1292 Logan, J. A., Staehelin, J., Megretskaia, I. A., Cammas, J. P., Thouret, V., Claude, H., De Backer, H.,
1293 Steinbacher, M., Scheel, H. E., Stübi, R., Fröhlich, M., and Derwent, R.: Changes in ozone over
1294 Europe: Analysis of ozone measurements from sondes, regular aircraft (MOZAIC) and alpine surface
1295 sites, *Journal of Geophysical Research*, 117, 1-23, 2012.

1296 Lombardozi, D., Levis, S., Bonan, G., and Sparks, J. P.: Predicting photosynthesis and transpiration
1297 responses to ozone: decoupling modeled photosynthesis and stomatal conductance, *Biogeosciences*,
1298 3113-3130, 2012.

1299 Lombardozi, D., Levis, S., Bonan, G., Hess, P. G., and Sparks, J. P.: The Influence of Chronic Ozone
1300 Exposure on Global Carbon and Water Cycles, *Journal of Climate*, 28, 292-305, 10.1175/jcli-d-14-
1301 00223.1, 2015.

1302 Long, S. P., Ainsworth, E. A., Leakey, A. D. B., Nosberger, J., and Ort, D. R.: Food for Thought: Lower-
1303 Than-Expected Crop Yield Stimulation with Rising CO₂ Concentrations, *Science*, 312, 1918-1921,
1304 10.1126/science.1114722, 2006.

1305 Löw, M., Herbinger, K., Nunn, A., Häberle, K.-H., Leuchner, M., Heerdt, C., Werner, H., Wipfler, P.,
1306 Pretzsch, H., and Tausz, M.: Extraordinary drought of 2003 overrules ozone impact on adult beech
1307 trees (*Fagus sylvatica*), *Trees*, 20, 539-548, 2006.

1308 Loya, W. M., Pregitzer, K. S., Karberg, N. J., King, J. S., and Giardina, C. P.: Reduction of soil carbon
1309 formation by tropospheric ozone under increased carbon dioxide levels., *Nature*, 425, 705-707,
1310 2003.

1311 Luysaert, S., Abril, G., Andres, R., Bastviken, D., Bellassen, V., Bergamaschi, P., Bousquet, P.,
1312 Chevallier, F., Ciais, P., Corazza, M., Dechow, R., Erb, K. H., Etiope, G., Fortems-Cheiney, A., Grassi, G.,
1313 Hartmann, J., Jung, M., Lathière, J., Lohila, A., Mayorga, E., Moosdorf, N., Njakou, D. S., Otto, J.,
1314 Papale, D., Peters, W., Peylin, P., Raymond, P., Rödenbeck, C., Saarnio, S., Schulze, E. D., Szopa, S.,
1315 Thompson, R., Verkerk, P. J., Vuichard, N., Wang, R., Wattenbach, M., and Zaehle, S.: The European
1316 land and inland water CO₂, CO, CH₄ and N₂O balance between 2001 and 2005, *Biogeosciences*, 9,
1317 3357-3380, 10.5194/bg-9-3357-2012, 2012.

1318 Massman, W. J.: A review of the molecular diffusivities of H₂O, CO₂, CH₄, CO, O₃, SO₂, NH₃, N₂O,
1319 NO, and NO₂ in air, O₂ and N₂ near STP, *Atmospheric Environment*, 32, 1111-1127,
1320 [http://dx.doi.org/10.1016/S1352-2310\(97\)00391-9](http://dx.doi.org/10.1016/S1352-2310(97)00391-9), 1998.

1321 Matyssek, R., Wieser, G., Ceulemans, R., Rennenberg, H., Pretzsch, H., Haberer, K., Löw, M., Nunn,
1322 A., Werner, H., and Wipfler, P.: Enhanced ozone strongly reduces carbon sink strength of adult beech
1323 (*Fagus sylvatica*)—Resume from the free-air fumigation study at Kranzberg Forest, *Environmental*
1324 *Pollution*, 158, 2527-2532, 2010a.

1325 Matyssek, R., Karnosky, D., Wieser, G., Percy, K., Oksanen, E., Grams, T., Kubiske, M., Hanke, D., and
1326 Pretzsch, H.: Advances in understanding ozone impact on forest trees: messages from novel
1327 phytotron and free-air fumigation studies, *Environmental Pollution*, 158, 1990-2006, 2010b.

1328 McLaughlin, S. B., Nosal, M., Wullschlegel, S. D., and Sun, G.: Interactive effects of ozone and climate
1329 on tree growth and water use in a southern Appalachian forest in the USA, *New Phytologist*, 174,
1330 109-124, 10.1111/j.1469-8137.2007.02018.x, 2007a.

1331 McLaughlin, S. B., Wullschlegel, S. D., Sun, G., and Nosal, M.: Interactive effects of ozone and climate
1332 on water use, soil moisture content and streamflow in a southern Appalachian forest in the USA,
1333 *New Phytologist*, 174, 125-136, 10.1111/j.1469-8137.2007.01970.x, 2007b.

1334 Medlyn, B. E., Badeck, F. W., De Pury, D. G. G., Barton, C. V. M., Broadmeadow, M., Ceulemans, R.,
1335 De Angelis, P., Forstreuter, M., Jach, M. E., Kellomaki, S., Laitat, E., Marek, M., Philippot, S., Rey, A.,
1336 Strassemeier, J., Laitinen, K., Liozon, R., Portier, B., Roberntz, P., Wang, K., and Jstbid, P. G.: Effects
1337 of elevated [CO₂] on photosynthesis in European forest species: a meta-analysis of model
1338 parameters, *Plant, Cell & Environment*, 22, 1475-1495, doi:10.1046/j.1365-3040.1999.00523.x, 1999.

1339 Medlyn, B. E., Barton, C. V. M., Broadmeadow, M. S. J., Ceulemans, R., De Angelis, P., Forstreuter,
1340 M., Freeman, M., Jackson, S. B., Kellomaki, S., Laitat, E., Rey, A., Roberntz, P., Sigurdsson, B. D.,
1341 Strassemeier, J., Wang, K., Curtis, P. S., and Jarvis, P. G.: Stomatal conductance of forest species
1342 after long-term exposure to elevated CO₂ concentration: a synthesis, *New Phytologist*, 149, 247-264,
1343 2001.

1344 Medlyn, B. E., Duursma, R. A., Eamus, D., Ellsworth, D. S., Prentice, I. C., Barton, C. V., Crous, K. Y., de
1345 Angelis, P., Freeman, M., and Wingate, L.: Reconciling the optimal and empirical approaches to
1346 modelling stomatal conductance, *Global Change Biology*, 17, 2134-2144, 2011.

1347 Mercado, L. M., Bellouin, N., Sitch, S., Boucher, O., Huntingford, C., Wild, M., and Cox, P. M.: Impact
1348 of changes in diffuse radiation on the global land carbon sink, *Nature*, 458, 1014-1017,
1349 http://www.nature.com/nature/journal/v458/n7241/supinfo/nature07949_S1.html, 2009.

1350 Mills, G., Hayes, F., Wilkinson, S., and Davies, W. J.: Chronic exposure to increasing background
1351 ozone impairs stomatal functioning in grassland species, *Global Change Biology*, 15, 1522-1533,
1352 2009.

1353 Mills, G., Pleijel, H., Braun, S., Büker, P., Bermejo, V., Calvo, E., Danielsson, H., Emberson, L.,
1354 Grünhage, L., Fernández, I. G., Harmens, H., Hayes, F., Karlsson, P.-E., and Simpson, D.: New stomatal

1355 flux-based critical levels for ozone effects on vegetation, *Atmospheric Environment*, 5064-5068,
1356 2011a.

1357 Mills, G., Hayes, F., Simpson, D., Emberson, L., Norris, D., Harmens, H., and BÜKer, P.: Evidence of
1358 widespread effects of ozone on crops and (semi-)natural vegetation in Europe (1990–2006) in
1359 relation to AOT40- and flux-based risk maps, *Global Change Biology*, 17, 592-613, 10.1111/j.1365-
1360 2486.2010.02217.x, 2011b.

1361 Mills, G., Harmens, H., Wagg, S., Sharps, K., Hayes, F., Fowler, D., Sutton, M., and Davies, B.: Ozone
1362 impacts on vegetation in a nitrogen enriched and changing climate, *Environmental Pollution*, 208,
1363 898-908, 2016.

1364 Norby, R. J., Wullschlegel, S. D., Gunderson, C. A., Johnson, D. W., and Ceulemans, R.: Tree responses
1365 to rising CO₂ in field experiments: implications for the future forest, *Plant, Cell and Environment*, 22,
1366 683-714, 1999.

1367 Norby, R. J., DeLucia, E. H., Gielen, B., Calfapietra, C., Giardina, C. P., King, J. S., Ledford, J., McCarthy,
1368 H. R., Moore, D. J. P., Ceulemans, R., De Angelis, P., Finzi, A. C., Karnosky, D. F., Kubiske, M. E., Lukac,
1369 M., Pregitzer, K. S., Scarascia-Mugnozza, G. E., Schlesinger, W. H., and Oren, R.: Forest response to
1370 elevated CO₂ is conserved across a broad range of productivity, *Proc. Natl. Acad. Sci. U. S. A.*, 102,
1371 18052-18056, 10.1073/pnas.0509478102, 2005.

1372 Nunn, A. J., Reiter, I. M., Häberle, K.-H., Langebartels, C., Bahnweg, G., Pretzsch, H., Sandermann, H.,
1373 and Matyssek, R.: Response patterns in adult forest trees to chronic ozone stress: identification of
1374 variations and consistencies, *Environmental Pollution*, 136, 365-369, 2005.

1375 O'Connor, F. M., Johnson, C. E., Morgenstern, O., Abraham, N. L., Braesicke, P., Dalvi, M., Folberth,
1376 G. A., Sanderson, M. G., Telford, P. J., Voulgarakis, A., Young, P. J., Zeng, G., Collins, W. J., and Pyle, J.
1377 A.: Evaluation of the new UKCA climate-composition model – Part 2: The Troposphere, *Geosci.*
1378 *Model Dev.*, 7, 41-91, 10.5194/gmd-7-41-2014, 2014.

1379 Paoletti, E., and Grulke, N. E.: Ozone exposure and stomatal sluggishness in different plant
1380 physiognomic classes, *Environmental Pollution*, 158, 2664-2671, 2010.

1381 Parrish, D. D., Law, K. S., Staehelin, J., Derwent, R., Cooper, O. R., Tanimoto, H., Volz-Thomas, A.,
1382 Gilge, S., Scheel, H. E., Steinbacher, M., and Chan, E.: Long-term changes in lower tropospheric
1383 baseline ozone concentrations at northern mid-latitudes, *Atmos. Chem. Phys.*, 12, 11485-11504,
1384 10.5194/acp-12-11485-2012, 2012.

1385 Parrish, D. D., Law, K. S., Staehelin, J., Derwent, R., Cooper, O. R., Tanimoto, H., Volz-Thomas, A.,
1386 Gilge, S., Scheel, H. E., Steinbacher, M., and Chan, E.: Lower tropospheric ozone at northern
1387 midlatitudes: Changing seasonal cycle, *Geophysical Research Letters*, 40, 1631-1636, 2013.

1388 Percy, K. E., Awmack, C. S., Lindroth, R. L., Kubiske, M. E., Kopper, B. J., Isebrands, J., Pregitzer, K. S.,
1389 Hendrey, G. R., Dickson, R. E., and Zak, D. R.: Altered performance of forest pests under atmospheres
1390 enriched by CO₂ and O₃, *Nature*, 420, 403-407, 2002.

1391 Royal-Society: Ground-level ozone in the 21st century: future trends, impacts and policy
1392 implications, *Science Policy Report 15/08*, 2008.

1393 Samuelsson, P., Jones, C. G., Willén, U., Ullerstig, A., Gollvik, S., Hansson, U., Jansson, C., Kjellström,
1394 E., Nikulin, G., and Wyser, K.: The Rossby Centre Regional Climate model RCA3: model description
1395 and performance, *Tellus A*, 63, 4-23, 2011.

1396 Saxe, H., Ellsworth, D. S., and Heath, J.: Tree and forest functioning in an enriched CO₂ atmosphere,
1397 *New Phytologist*, 139, 395-436, doi:10.1046/j.1469-8137.1998.00221.x, 1998.

1398 Schulze, E.-D., Ciais, P., Luyssaert, S., Schrupf, M., Janssens, I. A., Thiruchittampalam, B., Theloke, J.,
1399 Saurat, M., Bringezu, S., and Lelieveld, J.: The European carbon balance. Part 4: integration of carbon
1400 and other trace-gas fluxes, *Global Change Biology*, 16, 1451-1469, 2010.

1401 Schulze, E. D., Luyssaert, S., Ciais, P., Freibauer, A., Janssens, I. A., and et al.: Importance of methane
1402 and nitrous oxide for Europe's terrestrial greenhouse-gas balance, *Nature Geosci*, 2, 842-850,
1403 http://www.nature.com/ngeo/journal/v2/n12/supinfo/ngeo686_S1.html, 2009.

1404 Sicard, P., De Marco, A., Troussier, F., Renoua, C., Vas, N., and Paoletti, E.: Decrease in surface ozone
1405 concentrations at Mediterranean remote sites and increase in the cities, *Atmospheric Environment*,
1406 79, 705-715, 2013.

1407 Simpson, D., Benedictow, A., Berge, H., Bergström, R., Emberson, L. D., Fagerli, H., Flechard, C. R.,
1408 Hayman, G. D., Gauss, M., and Jonson, J. E.: The EMEP MSC-W chemical transport model—technical
1409 description, *Atmospheric Chemistry and Physics*, 12, 7825-7865, 2012.

1410 Simpson, D., Andersson, C., Christensen, J. H., Engardt, M., Geels, C., Nyiri, A., Posch, M., Soares, J.,
1411 Sofiev, M., and Wind, P.: Impacts of climate and emission changes on nitrogen deposition in Europe:
1412 a multi-model study, *Atmospheric Chemistry and Physics*, 14, 6995-7017, 2014a.

1413 Simpson, D., Arneth, A., Mills, G., Solberg, S., and Uddling, J.: Ozone—the persistent menace:
1414 interactions with the N cycle and climate change, *Current Opinion in Environmental Sustainability*, 9,
1415 9-19, 2014b.

1416 Sitch, S., Cox, P. M., Collins, W. J., and Huntingford, C.: Indirect radiative forcing of climate change
1417 through ozone effects on the land-carbon sink, *Nature*, 448, 791-794,
1418 http://www.nature.com/nature/journal/v448/n7155/supinfo/nature06059_S1.html, 2007.

1419 Sitch, S., Friedlingstein, P., Gruber, N., Jones, S. D., Murray-Tortarolo, G., Ahlström, A., Doney, S. C.,
1420 Graven, H., Heinze, C., Huntingford, C., Levis, S., Levy, P. E., Lomas, M., Poulter, B., Viovy, N., Zaehle,
1421 S., Zeng, N., Arneth, A., Bonan, G., Bopp, L., Canadell, J. G., Chevallier, F., Ciais, P., Ellis, R., Gloor, M.,
1422 Peylin, P., Piao, S. L., Le Quéré, C., Smith, B., Zhu, Z., and Myneni, R.: Recent trends and drivers of
1423 regional sources and sinks of carbon dioxide, *Biogeosciences*, 12, 653-679, 10.5194/bg-12-653-2015,
1424 2015.

1425 Sleutel, S., De Neve, S., and Hofman, G.: Estimates of carbon stock changes in Belgian cropland., *Soil
1426 Use and Management*, 19, 166-171, 10.1079/SUM2003187, 2003.

1427 Sun, G. E., McLaughlin, S. B., Porter, J. H., Uddling, J., Mulholland, P. J., Adams, M. B., and Pederson,
1428 N.: Interactive influences of ozone and climate on streamflow of forested watersheds, *Global Change
1429 Biology*, 18, 3395-3409, 10.1111/j.1365-2486.2012.02787.x, 2012.

1430 Tai, P. K. A., Val Martin, M., and Heald, C. L.: Threat to future global food security from climate
1431 change and ozone air pollution, *Nature Climate Change*, 4, 817 - 821, 2014.

1432 Talhelm, A. F., Pregitzer, K. S., Kubiske, M. E., Zak, D. R., Company, C. E., Burton, A. J., Dickson, R. E.,
1433 Hendrey, G. R., Isebrands, J. G., Lewin, K. F., Nagy, J., and Karnosky, D. F.: Elevated carbon dioxide
1434 and ozone alter productivity and ecosystem carbon content in northern temperate forests, *Global
1435 Change Biology*, 20, 2492-2504, 10.1111/gcb.12564, 2014.

1436 Tans, P., and Keeling, R.: NOAA/ESRL (www.esrl.noaa.gov/gmd/ccgg/trends/), Scripps Institution of
1437 Oceanography (scrippsco2.ucsd.edu/). , 2014.

1438 Tricker, P. J., Pecchiari, M., Bunn, S. M., Vaccari, F. P., Peressotti, A., Miglietta, F., and Taylor, G.:
1439 Water use of a bioenergy plantation increases in a future high CO₂ world, *Biomass and Bioenergy*,
1440 33, 200-208, 2009.

1441 Tuovinen, J.-P., Emberson, L., and Simpson, D.: Modelling ozone fluxes to forests for risk assessment:
1442 status and prospects, *Annals of Forest Science*, 66, 1-14, 2009.

1443 Tuovinen, J., Hakola, H., Karlsson, P., and Simpson, D.: Air pollution risks to Northern European
1444 forests in a changing climate, *Climate Change, Air Pollution and Global Challenges Understanding
1445 and Perspectives from Forest Research*, 2013.

1446 Uddling, J., Teclaw, R. M., Pregitzer, K. S., and Ellsworth, D. S.: Leaf and canopy conductance in aspen
1447 and aspen-birch forests under free-air enrichment of carbon dioxide and ozone, *Tree Physiology*, 29,
1448 1367-1380, 2009.

1449 van Vuuren, D. P., Edmonds, J., Kainuma, M., Riahi, K., Thomson, A., Hibbard, K., Hurtt, G. C., Kram,
1450 T., Krey, V., Lamarque, J.-F., Masui, T., Meinshausen, M., Nakicenovic, N., Smith, S. J., and Rose, S. K.:
1451 The representative concentration pathways: an overview, *Climatic Change*, 109, 5, 10.1007/s10584-
1452 011-0148-z, 2011.

1453 Verstraeten, W. W., Neu, J. L., Williams, J. E., Bowman, K. W., Worden, J. R., and Boersma, K. F.:
1454 Rapid increases in tropospheric ozone production and export from China, *Nature Geoscience* 8, 690-
1455 695, 2015.

1456 Vingarzan, R.: A review of surface ozone background levels and trends, *Atmospheric Environment*,
1457 38, 3431-3442, <https://doi.org/10.1016/j.atmosenv.2004.03.030>, 2004.

1458 Weedon, G. P., Gomes, S., Viterbo, P., Österle, H., Adam, J. C., Bellouin, N., Boucher, O., and Best, M.
1459 J.: The WATCH Forcing Data 1958-2001: a meteorological forcing dataset for land surface- and
1460 hydrological models. , WATCH Tech. Rep. 22, 41p (available at www.eu-watch.org/publications).
1461 2010.

1462 Weedon, G. P., Gomes, S., Viterbo, P., Shuttleworth, W. J., Blyth, E., Österle, H., Adam, J. C., Bellouin,
1463 N., Boucher, O., and Best, M.: Creation of the WATCH Forcing data and its use to assess global and
1464 regional reference crop evaporation over land during the twentieth century, *Journal of*
1465 *Hydrometeorology*, 12, 823-848, doi: 10.1175/2011JHM1369.1., 2011.

1466 Weedon, G. P.: Readme file for the "WFDEI" dataset.available at: [http://www.eu-](http://www.eu-watch.org/gfx_content/documents/README-WFDEI.pdf)
1467 [watch.org/gfx_content/documents/README-WFDEI.pdf](http://www.eu-watch.org/gfx_content/documents/README-WFDEI.pdf), 2013.

1468 Wild, O.: Modelling the global tropospheric ozone budget: exploring the
1469 variability in current models, *Atmospheric Chemistry and Physics*, 2643–2660, 2007.

1470 Wilkinson, S., and Davies, W. J.: Ozone suppresses soil drying-and abscisic acid (ABA)-induced
1471 stomatal closure via an ethylene-dependent mechanism, *Plant, Cell & Environment*, 32, 949-959,
1472 2009.

1473 Wilkinson, S., and Davies, W. J.: Drought, ozone, ABA and ethylene: new insights from cell to plant to
1474 community, *Plant, Cell & Environment*, 33, 510-525, 10.1111/j.1365-3040.2009.02052.x, 2010.

1475 Wittig, V. E., Ainsworth, E. A., and Long, S. P.: To what extent do current and projected increases in
1476 surface ozone affect photosynthesis and stomatal conductance of trees? A meta-analytic review of
1477 the last 3 decades of experiments, *Plant, Cell & Environment*, 30, 1150-1162, 10.1111/j.1365-
1478 3040.2007.01717.x, 2007.

1479 Wittig, V. E., Ainsworth, E. A., Naidu, S. L., Karnosky, D. F., and Long, S. P.: Quantifying the impact of
1480 current and future tropospheric ozone on tree biomass, growth, physiology and biochemistry: a
1481 quantitative meta-analysis, *Global Change Biology*, 15, 396-424, 10.1111/j.1365-2486.2008.01774.x,
1482 2009.

1483 Wullschleger, S. D., Gunderson, C. A., Hanson, P. J., Wilson, K. B., and Norby, R. J.: Sensitivity of
1484 stomatal and canopy conductance to elevated CO₂ concentration; interacting variables and
1485 perspectives of scale, *New Phytologist*, 153, 485-496, doi:10.1046/j.0028-646X.2001.00333.x, 2002.

1486 Young, P., Arneth, A., Schurgers, G., Zeng, G., and Pyle, J. A.: The CO₂ inhibition of terrestrial isoprene
1487 emission significantly affects future ozone projections, *Atmospheric Chemistry and Physics*, 9, 2793-
1488 2803, 2009.

1489 Young, P., Archibald, A., Bowman, K., Lamarque, J.-F., Naik, V., Stevenson, D., Tilmes, S., Voulgarakis,
1490 A., Wild, O., and Bergmann, D.: Pre-industrial to end 21st century projections of tropospheric ozone
1491 from the Atmospheric Chemistry and Climate Model Intercomparison Project (ACCMIP),
1492 *Atmospheric Chemistry and Physics*, 13, 2063-2090, 2013.

1493 Zaehle, S.: Terrestrial nitrogen–carbon cycle interactions at the global scale, *Philosophical*
1494 *Transactions of the Royal Society B: Biological Sciences*, 368, 20130125, 10.1098/rstb.2013.0125,
1495 2013.

1496 Zak, D. R., Pregitzer, K. S., Kubiske, M. E., and Burton, A. J.: Forest productivity under elevated CO₂
1497 and O₃: positive feedbacks to soil N cycling sustain decade-long net primary productivity
1498 enhancement by CO₂, *Ecology Letters*, 14, 1220-1226, 10.1111/j.1461-0248.2011.01692.x, 2011.

1499
1500
1501
1502

1503

1504

1505

1506